# Maintenance of epithelial traits and resistance to mesenchymal reprogramming promote proliferation in metastatic breast cancer

Laura Eichelberger[1,15], Massimo Saini[1,2,3,4,15], Helena Domínguez Moreno[5], Corinna Klein[2,3], Johanna M. Bartsch[1], Mattia Falcone[2,3], Manuel Reitberger[2,3], Elisa Espinet[2,3], Vanessa Vogel[2,3], Elisabeth Graf[6], Thomas Schwarzmayr[6], Tim-Matthias Strom[6], Mareike Lehmann[7], Melanie Königshoff[7], Nicole Pfarr[8], Roberto Würth[2,3], Elisa Donato[2,3], Simon Haas[2,3], Saskia Spaich[9], Marc Sütterlin[9], Andreas Schneeweiss[10], Wilko Weichert[11,12,13], Gunnar Schotta[5], Andreas Trumpp[2,3,12,*], Martin R. Sprick[2,3,12,*], and Christina H. Scheel[1,14,*]

1 Institute of Stem Cell Research, Helmholtz Center Munich, Neuherberg, Germany

2 Heidelberg Institute for Stem Cell Technology and Experimental Medicine (HI-STEM gGmbH), Heidelberg, Germany

3 Division of Stem Cells and Cancer, German Cancer Research Center (DKFZ), and DKFZ-ZMBH Alliance, Heidelberg, Germany

4 Present address: Department of Biomedicine, University Basel and University Hospital Basel, Basel, Switzerland

5 Biomedical Center (BMC) Munich, Ludwig-Maximilians-University (LMU) Munich, Planegg-Martinsried, Germany

6 Institute of Human Genetics, Helmholtz Center Munich, Neuherberg, Germany

7 Research Unit Lung Repair and Regeneration, Helmholtz Center Munich, Member of the German Center of Lung Research (DZL), Munich, Germany

8 Institute of Pathology, Technical University Munich (TUM), Munich, Germany

9 Department of Gynaecology and Obstetrics, University Women's Clinic, University Medical Centre Mannheim, Mannheim, Germany

10 National Center for Tumor Diseases, University Hospital and German Cancer Research Center, Heidelberg, Germany

11 Department of Pathology, Heidelberg University Hospital, Heidelberg, Germany

12 German Cancer Consortium (DKTK)

13 Present address: Institute of Pathology, Technical University Munich (TUM), Munich, Germany

14 Present address: Department of Dermatology, St. Josef Hospital, Ruhr-University Bochum, Bochum, Germany

15 These authors contributed equally: Laura Eichelberger, Massimo Saini

∗ These corresponding authors share equal senior-authorship: Christina H. Scheel, Martin R. Sprick, and Andreas Trumpp

**Correspondence to:**

Christina H. Scheel, christina.scheel@helmholtz-muenchen.de and

Martin R. Sprick, m.sprick@Dkfz-Heidelberg.de and

Andreas Trumpp, a.trumpp@Dkfz-Heidelberg.de

**Running title:**

Epithelial gene expression in EMT is required for breast cancer metastasis.

**Keywords:**

EPCAM, ZEB1, EMT, resistance, breast cancer, metastasis

**Abstract**

Despite important advances in the treatment of breast cancer, the 5-year survival rate for patients with distant metastasis remains less than 30%. Metastasis is a complex, multi-step process beginning with local invasion and ending with the outgrowth of systemically disseminated cells into actively proliferating metastases that ultimately cause the destruction of vital organs. It is this last step that limits patient survival and, at the same time, remains the least understood mechanistically. Here, we focus on understanding determinants of metastatic outgrowth using metastatic effusion biopsies from stage IV breast cancer patients. By modelling metastatic outgrowth through xenograft transplantation, we show that tumour initiation potential of patient-derived metastatic breast cancer cells across breast cancer subtypes is strongly linked to high levels of EPCAM expression. Breast cancer cells with high EPCAM levels are highly plastic and, upon induction of epithelial-mesenchymal transition (EMT), readily adopt mesenchymal traits while maintaining epithelial identity. In contrast, low EPCAM levels are caused by the irreversible reprogramming to a mesenchymal state with concomitant suppression of metastatic outgrowth. The ability of breast cancer cells to retain epithelial traits is tied to a global epigenetic program that limits the actions of EMT-transcription factor ZEB1, a suppressor of epithelial genes. Our results provide direct evidence that maintenance of epithelial identity is required for metastatic outgrowth while concomitant expression of mesenchymal markers enables plasticity. In contrast, loss of epithelial traits is characteristic of an irreversible mesenchymal reprogramming associated to a deficiency for metastatic outgrowth. Collectively, our data provide a framework for the intricate intercalation of mesenchymal and epithelial traits in metastatic growth.

72 **Introduction**

73 The outgrowth of macrometastases in vital organs causes almost all breast cancer
74 deaths[1]. Previously, it was shown that circulating tumour cells (CTCs) in blood of breast
75 cancer patients expressing the Epithelial Cell Adhesion Molecule (EPCAM) are
76 capable of initiating metastatic tumours *in vivo*[2]. However, it has been questioned
77 whether EPCAM is the most useful marker for CTCs since its expression is
78 downregulated when breast cancer cells undergo an epithelial-mesenchymal transition
79 (EMT)[3].

80 Experimental studies addressing the impact of EMT in different cancers have yielded
81 a wealth of controversial results. For example, it has been shown that the expression
82 of the EMT-inducer *Twist1* decreases proliferation of tumour cells, but increases their
83 abundance within the circulation[4]. Moreover, recent findings in a mouse model of
84 pancreatic carcinoma show that deletion of *Zeb1*, another EMT-transcription factor,
85 decreases invasion and lung colonization without affecting primary tumour growth,
86 suggesting that Zeb1 is crucial for tumour progression[5].

87 Other studies emphasize that a transient, rather than permanent expression of EMT-
88 transcription factors is crucial for the outgrowth of metastases[4,6,7]. This is supported by
89 the finding that most macroscopic metastases generated by carcinomas display an
90 epithelial morphology[8]. However, a strict requirement for EMT at any time during the
91 metastatic process is called into question by the finding that overexpression of micro
92 RNAs that inhibit EMT does not affect metastasis[9] and loss of *Twist1* and *Snai1*
93 expression in a pancreatic cancer mouse model does not change invasion and disease
94 progression[10].

95 More complication has recently arisen from the observation that tumour cells with an
96 intermediate, often termed hybrid epithelial-mesenchymal phenotype, are the most
97 competent in colonization and metastasis formation[11].

98 Some of this apparent controversy might be due to differences in the tissue- or cell-of
99 cancer origin. Nonetheless, the fundamental question how different phenotypes, i.e.
100 epithelial, mesenchymal, or hybrids arise, and how they contribute to metastatic
101 outgrowth remains poorly understood. To address this question in the context of breast
102 cancer, we examined the *in vivo* tumour-propagating ability of cancer cells derived from
103 effusion biopsies of metastatic breast cancer patients. We observed that, across
104 different breast cancer subtypes, EPCAM$^{high}$ cells were consistently more efficient in
105 establishing tumours in immunocompromised mice compared to EPCAM$^{low}$ cells.
106 These results guided subsequent mechanistic studies to understand why EPCAM$^{low}$
107 cells from metastatic biopsies failed to propagate the disease. Thereby we discovered
108 that a global epigenetic program prevents repression of epithelial genes in EPCAM$^{high}$
109 cells upon challenge by an EMT-inducing stimulus. Thus, our data suggest that the
110 ability to display epithelial-mesenchymal plasticity while maintaining epithelial identity
111 promotes metastatic outgrowth.
112
113 **Results**
114 **High EPCAM levels in patient-derived metastatic breast cancer cells correlate**
115 **with tumour propagation capacity**
116 To determine whether distinct tumour cell phenotypes contribute differently to
117 metastatic outgrowth, we used xenograft transplantation of cells from human cancers
118 as a proxy assay. For this purpose, we analysed liquid biopsies (pleural and ascitic
119 effusions) from stage IV breast cancer patients encompassing all major subtypes of
120 breast cancer (Supplementary Figure 1a). After excluding immune cells using CD45,
121 we identified three subpopulations of tumour cells present in these biopsies according
122 to cell surface levels of the Epithelial Cell Adhesion Molecule (EPCAM): EPCAM$^{high}$,
123 EPCAM$^{low}$, and EPCAM$^{neg}$ (Figure 1a, Supplementary Figure 1b). Next, we assessed

124 the tumour-initiating capacity (TIC) of each subpopulation *in vivo* by orthotopic
125 implantation in immunocompromised NSG mice to generate patient-derived xenografts
126 (PDX, Figure 1b). Strikingly, limiting dilution analysis revealed that across all subtypes,
127 $EPCAM^{high}$ cells were 30 times more efficient in generating tumours (TIC frequency:
128 $6.3x10^{-4}$) compared to $EPCAM^{low}$ cells ($2.1x10^{-5}$). $EPCAM^{neg}$ cells showed the lowest
129 efficiency in tumour generation ($1x10^{-6}$, Figure 1b). Importantly, the PDX-outgrowths
130 recapitulated the subtype of the primarily diagnosed tumour, as shown by subtype-
131 specific marker expression using immunohistochemistry (Supplementary Figure 1c).
132 Additionally, metastatic nodules in the lungs were exclusively found in mice injected
133 with $EPCAM^{high}$ cells (Figure 1b) and again expressed markers congruent with the
134 primary cancer subtype (Supplementary Figure 1d). Thus, these data suggest that
135 $EPCAM^{high}$ patient-derived breast cancer cells from metastatic sites preferentially
136 contribute to outgrowth compared to $EPCAM^{low}$ and $EPCAM^{neg}$ cells.
137 To take a closer look at breast cancer subtype-specific differences, effusion biopsies
138 were stratified according to oestrogen receptor (ER) status. Cells from patients with
139 ER-positive tumours ($ER^{+}$) showed the highest TIC frequency within the $EPCAM^{high}$
140 population ($1x10^{-5}$) compared to $EPCAM^{low}$ ($5.6x10^{-5}$), while the $EPCAM^{neg}$ population
141 lacked detectable TICs (Figure 1b). In biopsies from patients with ER-negative tumours
142 ($ER^{-}$), all populations initiated tumours to a certain extent (Figure 1b), consistently with
143 a higher degree of phenotypic plasticity previously observed in $ER^{-}$ liquid biopsies[12].
144 Nonetheless, we observed a 15 times higher TIC frequency in $EPCAM^{high}$ cells
145 ($3.6x10^{-3}$) compared to $EPCAM^{low}$ cells ($2.4x10^{-4}$), and the lowest TIC frequency in
146 $EPCAM^{neg}$ cells ($9.1x10^{-4}$, Figure 1b).
147 Since metastatic effusion biopsies are derived from body cavities lined with
148 mesothelium, contamination with sloughed-off, normal mesothelial cells could
149 potentially provide a simple explanation for the lower TIC frequency in $EPCAM^{low}$ and

150 EPCAM$^{neg}$ cell populations. To test this possibility, we assessed the mutational
151 spectrum in EPCAM-sorted subpopulations by using panel-based targeted sequencing
152 covering 50 commonly mutated breast cancer genes. Thus, 13 different somatic
153 mutations were detected and their allelic frequency evaluated in each subpopulation
154 (Figure 1c). This analysis revealed that across subtypes, the frequency of mutated
155 alleles in the EPCAM$^{neg}$ population was significantly lower compared to the EPCAM$^{low}$
156 ($p=0.039$) or EPCAM$^{high}$ populations ($p=0.0098$, Figure 1c), indicating that the
157 EPCAM$^{neg}$ population contained a significant amount of non-tumour cells. By contrast,
158 EPCAM$^{high}$ and EPCAM$^{low}$ populations showed comparable allelic frequencies for all
159 mutations detected.
160 Together, these results suggest that the observed differences in TIC frequency in the
161 EPCAM$^{neg}$ population might arise from contamination with normal cells, whereas the
162 observed differences between EPCAM$^{high}$ and EPCAM$^{low}$ populations originate from
163 qualitative differences between these populations. Since we observed highly similar
164 mutation profiles between these populations, we speculated that the observed
165 differences in TIC frequency might arise from differences in epigenetic rather than
166 genetic cellular programs.
167 To further explore this hypothesis, we performed RNA-sequencing of freshly sorted
168 EPCAM subpopulations from an ER$^{+}$ and an ER$^{-}$ patient. Among larger and non-
169 redundant gene set collections, one of the most enriched features in EPCAM$^{low}$ cells
170 was the EMT process (Figure 1d, Supplementary Figure 1e). By contrast, EPCAM$^{high}$
171 cells were enriched for multiple features associated with an active cell cycle, oxidative
172 phosphorylation, MYC targets and in general, pathways associated with cell growth
173 (Figure 1d, Supplementary Figure 1f).
174 This result supported the conclusion derived from xenograft transplantation: in
175 metastatic effusion biopsies, EPCAM expression serves as a marker distinguishing

176 between disease-propagating, actively growing tumour cells and less proliferative
177 subpopulations. Moreover, RNA-sequencing pointed us towards EMT programs as a
178 potential underlying mechanism for the reduction in TICs we observed in the EPCAM$^{low}$
179 cells.
180

181 **Contrasting responses to an EMT-inducing stimulus generate morphological**
182 **and functional heterogeneity in breast cancer cells**

183 To investigate whether EMT programs in breast cancer cells contribute to a
184 suppression of metastatic outgrowth and to explore the role of epithelial traits, we
185 induced EMT in epithelial breast cancer cells under defined conditions. To do so, we
186 used immortalized human mammary epithelial cells (HMLE) engineered to express a
187 conditional *Twist1*-ER (HMLE-Twist1-ER) activatable by Tamoxifen (TAM)
188 treatment[7,13].
189 After 21 days of persistent Twist1-activation all cells, based on morphology, appeared
190 to have trans-differentiated from an epithelial to a mesenchymal phenotype
191 (Supplementary Figure 2a). Indeed, analysis of cell-surface EPCAM expression after
192 Twist1-activation revealed that most cells had lost EPCAM cell surface expression.
193 However, a minor subset of cells continued to express EPCAM (Figure 2a,
194 Supplementary Figure 2c), indicating that the latter subset of cells was resistant to
195 EMT-induction. To functionally address this heterogeneity, we prospectively sorted
196 EPCAM$^{neg}$ and EPCAM$^{pos}$ cells (Figure 2a). Sorted cells were transferred to
197 Tamoxifen-free conditions for 10 days (+TAM 21d/-TAM 10d) to reproduce the effect
198 of a transient EMT stimulus, as it is thought to take place during tumour progression[14].
199 Based on morphology and expression of markers such as E-cadherin (*CDH1*),
200 EPCAM$^{neg}$ cells could be identified as a population that remained mesenchymal even
201 after cessation of Twist1-activation. By contrast, EPCAM$^{pos}$ cells displayed an

202 epithelial phenotype, thus showing insensitivity to the EMT-inducing stimulus provided
203 by Twist1-activation (Figure 2b, c, Supplementary Figure 2b). Next, we tested the
204 ability of EPCAM$^{pos}$ and EPCAM$^{neg}$ cells to generate organoids in a three-dimensional
205 collagen gel-based organoid assay to mimic more physiological growth conditions[7,15].
206 Strikingly, only EPCAM$^{pos}$ cells proliferated, whereas EPCAM$^{neg}$ cells failed to
207 generate organoids (Figure 2d, e).
208 Together, these results showed that contrasting cellular responses to an EMT-inducing
209 stimulus create heterogeneity with respect to EPCAM-expression in a breast cancer
210 cell line model similar to what we encountered in metastatic effusion biopsies (Figure
211 1). Moreover, these data suggest that a proportion of breast cancer cells can resist
212 induction of EMT and maintain epithelial properties, whereas cells that undergo
213 irreversible EMT lose their ability to proliferate in a three-dimensional environment.
214

215 **Single-cell level analysis confirms that breast cancer cells either intrinsically**
216 **resist EMT-induction or enter a stable, mesenchymal cell state**

217 Based on these data, we set out to understand why some cells appeared to be more
218 susceptible to EMT than others. For this purpose, we generated several single-cell
219 clones (SCCs, Supplementary Figure 3a) from the HMLE-Twist1-ER bulk population
220 and treated the clones with TAM independently to assess the competence for EMT at
221 the single-cell level. Again, we observed that only a subset of single-cell clones (SCCs)
222 underwent EMT (42 of 58, 72%), indicated by a gain of mesenchymal traits and the
223 concurrent loss of epithelial traits (M-SCCs: M1-3, Figure 3a, b). The remaining SCCs
224 (16 of 58, 28%) failed to undergo EMT and remained epithelial (E-SCCs: E1-3, Figure
225 3a, b). Importantly, Twist1 nuclear localisation and expression levels, as well as
226 transcript levels of the direct target gene *WNT5A*[16] were quantitatively comparable in

227 all clones (Supplementary Figure 3b-d), ruling out variable Twist1 expression levels as
228 the reason for the differences in susceptibility for EMT induction.
229 In detail, Twist1-activation led to a complete loss of surface EPCAM expression in M-
230 SCCs, while we observed only a minor shift in E-SCCs (Figure 3c, d). Moreover,
231 expression of E-cadherin (CDH1) was maintained in E-SCCs, but not M-SCCs (Figure
232 3b, d, e). By contrast, expression of mesenchymal markers such as Vimentin (VIM)
233 was upregulated upon Twist1-activation in both E-SCCs and M-SCCs to a similar
234 extent (Figure 3b, d, e). Thus, E-SCCs adopted a transient hybrid phenotype during
235 Twist1-activation, characterized by concomitant expression of epithelial and
236 mesenchymal markers.
237 By contrast, epithelial markers were permanently downregulated in M-SCCs with
238 concomitant high expression levels of mesenchymal genes (Supplementary Figure 3e,
239 f). Thus, M-SCCs did not undergo a mesenchymal-epithelial transition (MET) following
240 inactivation of Twist1, but persisted in a mesenchymal state.
241 Importantly, the contrasting responses to Twist1 in E-SCCs and M-SCCs did not simply
242 reflect differences in kinetics to EMT-induction: during prolonged Twist1-activation for
243 21 or 28 days, E-SCCs still maintained an epithelial phenotype and the expression of
244 epithelial markers such as E-cadherin (*CDH1)* (Supplementary Figure 3g, h). This
245 result suggests a strong protection of epithelial traits in E-SCCs that cannot be
246 overcome by long-term activation of an EMT-inducing stimulus.
247
248 **Resistance to complete EMT correlates with the ability of breast cancer cells to**
249 **proliferate in a three-dimensional environment**
250 Next, we wished to determine whether resistance to EMT again correlated with the
251 capacity for growth in a three-dimensional environment. To do so, individual SCCs
252 were plated in a collagen gel-based organoid assay[7,15]. Thereby, we observed that

253 prior to an EMT-stimulus E-SCCs and M-SCCs formed epithelial organoids expressing
254 E-cadherin with similar frequency (Figure 3f, g). However, when E-SCCs and M-SCCs
255 were plated into the organoid assay after 14 days of transient Twist1-activation, only
256 E-SCCs generated epithelial organoids, as observed in breast cancer metastases[8]. By
257 contrast, M-SCCs remained in the collagen gel as single cells and failed to initiate
258 proliferation (Figure 3f, g).
259 To further explore this deficiency in proliferation and approximate conditions during
260 metastatic outgrowth, we tested the growth of E-SCCs and M-SCCs on precision-cut
261 lung slices (PCLS), which allow analysis of 3D-lung tissue architecture *ex vivo*[17]. For
262 this purpose, PCLS were incubated for 5 days in Tamoxifen-free conditions with
263 $GFP^{pos}$ E-SCCs or M-SCCs that were either untreated or treated with TAM for 14 days.
264 Strikingly, even before Twist1-activation, E-SCCs were 1.6-fold more efficient in
265 colonizing the PCLS (Figure 3h, i). However, after transient Twist1-activation, the
266 ability of M-SCCs to proliferate on the lung slices decreased further and E-SCCs
267 colonized the PCLS 3.9-fold more efficient than M-SCCs (Figure 3h, i).
268 Together, these data further supported our observation that resistance to complete
269 EMT through maintenance of epithelial features promotes the ability of breast cancer
270 cells to initiate proliferation in different three-dimensional environments, possibly
271 correlating with the capacity for metastatic outgrowth.
272 Since HMLE cells are not tumorigenic in immunocompromised mice we prospectively
273 sorted the $EPCAM^{pos}$ and $EPCAM^{neg}$ subpopulations of SUM-149PT breast cancer
274 cells (Figure 3j, k) to evaluate their *in vivo* metastatic potential. For this, we injected
275 these populations into the hindleg femurs of NSG mice as previously described[2] in
276 order to evaluate metastasis-initiating activity in the bone, the most frequent site of
277 metastasis in breast cancer. Indeed, $EPCAM^{pos}$ cells generated bone metastases after

278 20 weeks of observation, while EPCAM$^{neg}$ cells failed to produce metastases (Figure
279 3l).
280 Together, data from different experimental models *in vitro* and *in vivo* support the idea
281 that the occurrence of complete EMT negatively impacts metastatic outgrowth whereas
282 the maintenance of epithelial features promotes metastasis.
283
284 **Global chromatin changes during transient EMT-induction define EMT-**
285 **resistance versus -susceptibility**
286 To investigate the mechanistic basis for EMT-resistance versus -susceptibility, we
287 again turned to E-SCCs and M-SCCs derived from HMLE-Twist1-ER cells.
288 Specifically, we wished to determine whether the contrasting responses of SCCs to
289 Twist1-activation could be observed at an epigenetic regulatory level. For this purpose,
290 we performed ATAC-sequencing in conjunction with RNA-sequencing in three E-SCCs
291 and three M-SCCs before Twist1-activation (1), after 7 (2) and 14 days of Twist1-
292 activation (3), and after 14 days of Twist1-activation followed by 7 days of Twist1-
293 deactivation (4).
294 Principal component analysis (PCA) revealed a comparable landscape of chromatin
295 accessibility in E-SCCs and M-SCCs before Twist1-activation (Figure 4a). However,
296 both at 7 and 14 days after Twist1-activation, M-SCCs harboured the greatest variation
297 in chromatin accessibility compared to all other conditions, which was evident in
298 changes that created a shift on the PC1 axis (Figure 4a). In contrast, during Twist1-
299 activation, changes observed in E-SCCs created a shift on the PC2 axis,
300 corresponding to comparatively minor variance (Figure 4a).
301 Remarkably, upon Twist1 deactivation (+TAM 14d/-TAM 7d), changes in chromatin
302 accessibility were reversed in E-SCCs but not in M-SCCs (Figure 4a). Thus, the
303 dynamics of chromatin accessibility in E-SCCs and M-SCCs mirrored our observations

304 that during transient Twist1-activation, E-SCCs can temporarily acquire a hybrid
305 phenotype, whereas M-SCCs remain in a stable mesenchymal state. This was further
306 corroborated by focusing on the loci of epithelial genes such as *EPCAM* and *CDH1*:
307 here, we observed that before Twist1-activation, both loci were similarly accessible.
308 However, during Twist1-activation, access to both loci was lost in M-SCCs, but not E-
309 SCCs (Figure 4b). RNA-sequencing revealed comparable dynamics with respect to
310 changes in transcript abundance (Supplementary Figure 4a), indicating that changes
311 observed at the transcript level can be traced back to chromatin accessibility and *vice*
312 *versa*.
313 Together, these results reveal that global changes in chromatin accessibility developed
314 during Twist1-activation are less dramatic and reversible in E-SCCs compared to M-
315 SCCs. These changes in chromatin accessibility correlate with differences in gene
316 expression and, as a corollary, the functional differences we observed between E-
317 SCCs and M-SCCs after transient Twist1-activation.
318 In order to pinpoint transcription factors (TFs) involved in these transitions, we
319 performed peak clustering of the ATAC-sequencing data. By doing so, we confirmed
320 close clustering of E-SCCs and M-SCCs before Twist1-activation. After Twist1-
321 activation, E-SCCs continued to cluster closer with the untreated condition, whereas
322 treated M-SCCs formed a distinct cluster (Figure 4c). Detailed analysis revealed three
323 different types of changes in chromatin accessibility during Twist1-activation: loci
324 previously not accessible that become accessible in both M-SCCs and E-SCCs (c3,
325 c4), loci becoming accessible only in M-SCCs, but not E-SCCs (c6, c7, c11, c9), and
326 loci losing accessibility in M-SCCs, but not E-SCCs (c2, c12, c5, c8, c1, c10, Figure
327 4c). Of note, the latter clusters contained the loci of epithelial genes, such as *CDH1*
328 and *EPCAM*. Homer *de novo* TF motif analysis of combined clusters revealed specific
329 motifs representing each cluster type (Figure 4d, Supplementary Figure 4b).

330 Importantly, the results included several motifs that have been previously shown to be
331 enriched in cells undergoing EMT in mice *in vivo*[11]. For example, this included loss of
332 accessibility in M-SCCs for a p53/p73/p63 binding motif, a gain in accessibility for basic
333 leucine zipper TF motifs in M-SCCs, and TEAD and AP-1 motifs as well as a TCF4
334 binding motif becoming newly accessible upon Twist1-activation in both M-SCCs and
335 E-SCCs (Figure 4d, Supplementary Figure 4b). Interestingly, TCF4 binds to an E-box
336 motif and was shown to interact with TWIST1[18,19]. Additionally, the same cluster type
337 revealed enrichment of a consensus Twist binding motif (Supplementary Figure 4b).
338 The observation that Twist motifs enrich in loci commonly accessible in both E-SCCs
339 and M-SCCs is in line with our observations that Twist1 appeared to be similarly active
340 in E-SCCs and M-SCCs with respect to specific target loci that are actively transcribed
341 (e.g. *WNT5A*).
342 Together, these data suggest that Twist1 is indeed active in both E-SCCs and M-SCCs
343 and that the different cellular responses to Twist1 activation are not merely the result
344 of Twist1 not functioning as a transcription factor in these cells. As a corollary, our
345 results indicate that the events leading to EMT-resistance or -susceptibility may occur
346 downstream of Twist1-binding to chromatin.
347 To further investigate this hypothesis, we focused on regions where chromatin
348 accessibility was lost in M-SCCs but not E-SCCs during Twist1-activation (c2, c12, c5,
349 c8, c1, c10, Figure 4c). Here, *de novo* binding motif analysis revealed an enrichment
350 for ZEB1 and ZEB2 motifs (Figure 4d). ZEB1 is known as a key EMT-transcription
351 factor downstream of Twist1 that represses the expression of epithelial genes, such as
352 E-cadherin (*CDH1*)[20] and *EPCAM*[21]. Additionally, we observed enrichment of GRHL1
353 and GRHL2 motifs in clusters that become accessible exclusively in M-SCCs during
354 Twist1-activation (Figure 4d). Importantly, grainy-head like factors (GRHL1-3) are

355 known to prime epithelial enhancers for transcriptional activation[22]. Moreover, *GRHL2*
356 expression is controlled by ZEB1 in a negative feedback-loop[23].
357 Together, these results suggest ZEB and/or GRHL as mediators determining whether
358 breast cancer cells undergo irreversible EMT or resist trans-differentiation.
359
360 **ZEB1 is necessary, but not sufficient to overcome EMT-resistance in breast**
361 **cancer cells**
362 Next, we looked more closely at the RNA-sequencing results that were obtained
363 concomitantly with ATAC-sequencing data at different time points of Twist1-activation.
364 Expression of *GRHL1* and *GRHL2* was downregulated during EMT in M-SCCs but not
365 E-SCCs. Specifically, high expression levels of *GRHL2* were maintained in E-SCCs,
366 but expression was strongly downregulated in M-SCCs (Figure 5a). In support of our
367 data, GRHL2 was recently shown to be a pioneering transcription factor that maintains
368 the chromatin of epithelial genes in an open state[22,24]. Moreover, when analysing
369 expression levels of *ZEB1* and *ZEB2*, we also observed a clear difference between E-
370 SCCs and M-SCCs that was particularly pronounced for *ZEB1* (Figure 5b, d). With
371 respect to kinetics, *ZEB1* was upregulated in E-SCCs after 14 days of Twist1-
372 activation, whereas in M-SCCs an upregulation could already be observed after 7 days
373 (Figure 5b, d). Additionally, after 14 days of Twist1-activation, *ZEB1* expression levels
374 were 2.9-fold higher in M-SCCs compared to E-SCCs (Figure 5c). These data were in
375 line with the observation that *ZEB1* expression was also higher in sorted EPCAM$^{neg}$
376 HMLE-Twist1-ER cells compared to sorted EPCAM$^{pos}$ cells (Figure 2c). Next, we
377 determined the expression of ZEB1 downstream targets such as *OVOL2* and *MIR200*-
378 family members, which function in negative feedback loops with ZEB1[20,25,26]. Indeed,
379 transcription of both *OVOL2* and *MIR200*-family members was downregulated in M-
380 SCCs, but not E-SCCs during transient Twist1-activation, suggesting that negative

381 feedback loops restricting ZEB1-activity remained active in E-SCCs, but were disabled
382 in M-SCCs (Figure 5c, Supplementary Figure 5a). In line with these data, epithelial
383 ZEB1-target genes such as *OVOL2* and *CDH1* remained repressed after transient
384 Twist1-activation in M-SCCs, whereas the expression of mesenchymal genes such as
385 *VIM* and *FN1* remained high (Supplementary Figure 3f). Strikingly, prolonged Twist1-
386 activation could not break these feedback loops and overcome EMT-resistance in E-
387 SCCs (Supplementary Figure 3h).
388 Together these results suggest that differences in ZEB1-activation and -levels are
389 implicated in the contrasting responses to EMT-induction in E-SCCs and M-SCCs. In
390 detail, Twist1-activation resulted in higher *ZEB1* expression in EMT-susceptible cells,
391 which in turn lead to the transcriptional repression of epithelial genes such as *EPCAM*,
392 *CDH1*, *OVOL2*, and *MIR200*-family members. By contrast, E-SCCs resisted
393 repression of epithelial genes, which also served to restrict ZEB1-activation since
394 many of these genes are known to function in a direct negative feedback loop.
395 To test, whether *ZEB1* was necessary for the irreversible EMT observed in M-SCCs,
396 we generated M-SCC *ZEB1* knockout (KO) single-cell clones (Figure 5e, f,
397 Supplementary Figure 5b, c). Upon Twist1-activation through TAM treatment, *ZEB1*
398 KO clones indeed failed to undergo EMT in contrast to control cells, as evidenced by
399 the maintenance of downstream epithelial markers like *CDH1* and *OVOL2* (Figure 5e,
400 f, Supplementary Figure 5d).
401 These results demonstrate that activation of *ZEB1* is required for EMT and the
402 resultant trans-differentiation from an epithelial to a mesenchymal phenotype
403 alongside with the repression of epithelial markers. Therefore, inefficient induction of
404 *ZEB1* expression in E-SCCs might explain the observed resistance to EMT-induction.
405 Next, we wished to determine whether *ZEB1* overexpression (OE) was sufficient to
406 overcome EMT-resistance in E-SCCs. Therefore, we generated E-SCC single-cell

407 clones conditionally overexpressing *ZEB1*. Treatment with doxycycline and
408 concomitant induction of *ZEB1* expression for 7 days led to EMT in *ZEB1* OE clones
409 as indicated by morphology and downregulation of its targets *OVOL2*, *CDH1*, and
410 EPCAM in contrast to a control clone, which remained resistant to EMT (Figure 5g, h,
411 Supplementary Figure 5e, f). However, upon doxycycline withdrawal for 14 days, *ZEB1*
412 OE clones reverted to an epithelial phenotype and regained expression of epithelial
413 markers such as *CDH1* and *OVOL2* (Figure 5g, Supplementary Figure 5e).
414 Thus, even though we observed a transient downregulation of epithelial traits in E-
415 SCCs, *ZEB1* overexpression was not sufficient for trans-differentiation of EMT-
416 resistant cells into an irreversible mesenchymal state.
417 Together, these data suggest that a globally acting epigenetic mechanism exists in
418 EMT-resistant cells that prevents ZEB1 from repressing epithelial genes independently
419 of *ZEB1* expression levels. The resultant epigenetic stabilization of cellular identity
420 promotes plasticity by enabling cells to maintain an epithelial identity while co-
421 expressing mesenchymal markers. Moreover, it appears that initiation of proliferation
422 in different settings that mimic metastatic outgrowth is directly connected to epithelial
423 identity, whereas this capacity is suppressed by loss of epithelial traits through
424 mesenchymal reprogramming.
425
426 **Discussion**
427 In this study, we report that heterogeneity exists with respect to EPCAM levels which
428 range from low to high in patient-derived metastatic breast cancer samples obtained
429 from liquid biopsies. We observed that the ability to initiate tumours upon
430 xenotransplantation was enriched in EPCAM$^{high}$ compared to EPCAM$^{low}$ patient-
431 derived metastatic breast cancer cells. The transcriptome of EPCAM$^{low}$ breast cancer
432 cells showed a correlation with EMT related genes, suggesting that the maintenance

433 of an epithelial identity in EPCAM$^{high}$ breast cancer cells promotes metastatic
434 outgrowth of these cells (Figure 6a). Indeed, using an experimental system based on
435 human breast cancer cells, we observed that some cells actively resist EMT-induction.
436 This resistance corresponded to a global epigenetic mechanism serving to restrict the
437 activity of the transcriptional repressor ZEB1 and preventing the loss of chromatin
438 accessibility at loci containing epithelial genes including E-cadherin (*CDH1*, Figure 6b).
439 Indeed, expression of E-cadherin has recently been shown to directly promote
440 metastatic outgrowth[27].
441 Importantly, our data not only supports the concept that epithelial features promote
442 metastatic outgrowth, but reveal that these features are actively maintained. On the
443 flip side, we show that breast cancer cells that are susceptible to repression of epithelial
444 features undergo irreversible EMT, a process characterized by high levels of ZEB1
445 and concomitantly, reduced chromatin accessibility over widespread genomic regions
446 that include genes determining epithelial identity and, at the same time restricting
447 ZEB1-activity via negative feedback loops (Figure 6b). When such cells with
448 compromised epithelial identity are either derived from breast cancer metastatic
449 biopsies or cell lines, we consistently observe a reduced ability to initiate proliferation
450 in different settings that mimic metastatic outgrowth.
451 In conclusion, our study combines evidence from multiple models of the human
452 disease, consistently indicating that the preservation of epithelial gene expression
453 during EMT-induction is a fundamental mechanism for metastatic propagation of
454 breast cancers, whereas EMT-susceptibility results in a permanent mesenchymal state
455 coupled to growth arrest.
456 Our findings are supported by a recent study showing that spontaneous epithelial-
457 mesenchymal trans-differentiation in a subset of HMLE-Ras cells residing in a
458 mesenchymal state reduces tumorigenicity[28]. This study, together with a

459 comprehensive analysis of EMT-transition states in murine models of mammary and
460 cutaneous squamous carcinoma also suggests that a hybrid epithelial-mesenchymal
461 phenotype is required for tumour progression[11,28]. However, neither the work by
462 Padmanaban et al.[27] nor our study is necessarily in conflict with these data. On the
463 contrary, our work suggests a possible mechanistic basis for a hybrid epithelial-
464 mesenchymal state, defined by active maintenance of epithelial gene expression and
465 concomitant upregulation of mesenchymal markers. Moreover, our data suggest that
466 transient entrance into such a hybrid state might enable metastatic progression, which
467 is in line with several other studies[4,6,7].
468 However, when focusing on the last step of metastasis, i.e. the outgrowth of
469 disseminated cells into actively growing macrometastases, our data support a model
470 suggesting that epithelial features, not necessarily a hybrid phenotype, drive metastatic
471 outgrowth, as epithelial identity appears to be tied to cellular programs that govern
472 proliferation. This is particularly important in light of the fact that it is this last step of
473 metastatic progression that limits patient survival. In line with that, others hypothesized
474 that repression of EMT will not affect outgrowth of metastases, as epithelial tumour
475 cells with high proliferative capacity outcompete cells that have undergone an EMT[9].
476 One obvious question arising from our data is why EPCAM$^{low}$ breast cancer cells are
477 present in metastatic effusion biopsies in the first place, if they are not capable of
478 propagating the disease. In this context, it has been previously observed that in primary
479 tumours, mesenchymal cancer cells might cooperate with epithelial cancer cells to
480 enable the systemic dissemination of both cell populations[29]. Therefore, one could
481 hypothesize that EPCAM$^{low}$ cells might promote the systemic dissemination and
482 subsequent growth of EPCAM$^{high}$ breast cancer cells.
483 Additionally, we need to keep in mind that patients within this study were treated with
484 chemotherapy. As it was shown that mesenchymal, EMT cells resist chemotherapy

485 whereas epithelial, non-EMT tumour cells are sensitive to chemotherapy[9], the
486 presence of mesenchymal breast cancer cells at the metastatic site could also be
487 explained by their resistance to the therapy. These cells could potentially remain as
488 dormant population and thereby counterbalance their proliferative disadvantage.
489 Because of that, we would like to add an important caveat to these considerations: our
490 data suggest that EMT might create heterogeneity with respect to proliferative
491 capacity. Although our data suggest that complete EMT, and hence, the resultant
492 growth suppression might be permanent, it will nonetheless be important to take the
493 observed cellular heterogeneity into account when developing new treatment
494 strategies for metastatic breast cancer.
495 Most importantly, our results strongly support the emerging evidence linking epithelial
496 identity to metastatic outgrowth. Additionally, our data provide evidence for a globally
497 acting, epigenetic mechanism serving to render cells resistant against mesenchymal
498 reprogramming and thereby serve to actively maintain and anchor epithelial features
499 in the metastases.

500 **Methods**

501 **Clinical specimens**

502 Pleural and ascitic effusions were obtained from post-menopausal stage IV patients
503 admitted to the Division of Gynecologic Oncology, National Centre for Tumor Diseases
504 and the Women's Clinic of the Mannheim University Hospital. The study was approved
505 by the ethical committee of the University of Heidelberg (case number S295/2009) and
506 University of Mannheim (2010-024238-46). All samples were transferred to the
507 laboratory no later than 1 hour after thoracentesis or laparocentesis and processed to
508 extract cancer cells as previously described[30]. Patient's diagnostic information and
509 clinical disease characteristics are described in detail in Table 1.

510

511 **Xenograft assay for patient-derived metastatic breast cancer cells**

512 Female NOD.Cg-Prkdc$^{scid}$ Il2rg$^{tm1Wjl}$/SzJ (NSG) mice were transplanted at 6 to 8 weeks
513 of age. A suspension of FACS-purified cells in sterile PBS was combined to growth
514 factor-reduced Matrigel (BD) in a 1:1 ratio and then injected in the 4$^{th}$ or the 5$^{th}$
515 mammary fat pad. All mice received subcutaneous implantation of beta-estradiol as
516 solid pellets (Innovative Research of America) with modalities that were already
517 described[2]. Engraftment of cancer cells and growth *in vivo* was monitored by regular
518 palpation of the implantation site. Animal care and procedures followed the German
519 legal regulations and were previously approved by the governmental review board of
520 the state of Baden-Württemberg, operated by the local Animal Welfare Office
521 (Regierungspräsidium Karlsruhe) under the license number G240-11.

522

523 **Immunohistochemical analysis of tumour xenografts**

524 Tumour lesions generated in mice and metastatic lungs were freshly collected upon
525 necropsy and embedded in paraffin for downstream histological inspections. Sections

526 were obtained, processed and stained as described[31]. For immunohistochemistry, the
527 following antibodies were used: anti-human Ki-67 (DAKO, clone Ki-67), anti-oestrogen
528 receptor alpha (Thermo Fisher Scientific, clone SP1), anti-progesterone receptor
529 (DAKO, clone PgR636), anti-HER2 (DAKO, polyclonal serum A0485), anti-CDH1
530 (DAKO, clone M3612), and anti-Vimentin (DAKO, clone M0725).
531
532 **Targeted next-generation sequencing of somatic mutations**
533 Genomic DNA was extracted from FACS-purified cancer cells and matched germline
534 controls ($CD45^+$ white blood cells purified by FACS sorting from the same metastatic
535 effusion). The concentration of nucleic acids was assessed by fluorimetric
536 measurement through QuBit 3.0 and the amount of amplifiable DNA (sequencing-
537 grade quality) was determined using a quantitative assay (TaqMan RNAseP detection
538 assay) on a StepOnePlus instrument (both: Thermo Fisher Scientific). Samples were
539 amplified using a custom-designed gene panel for breast cancer[32] covering the most
540 recurrent mutations[33]. Library preparation and sequencing were performed using the
541 multiplex PCR-based Ion Torrent AmpliSeq™ technology (Thermo Fisher Scientific)
542 and Ion S5XL technology, with procedures already described[34].
543
544 **RNA-sequencing of patient-derived metastatic breast cancer cells**
545 RNA extraction was carried out from 40,000 FACS-sorted cells using ARCTURUS
546 PicoPure RNA isolation kit (Thermo Scientific, Cat. KIT0204). RNA quality was
547 assessed using BioAnalyzer 2100 (Agilent). Libraries were prepared from 1 µg of total
548 RNA using a TruSeq Stranded Total RNA Kit with Ribo-Zero Human/Mouse/Rat
549 (Illumina) according to the manufacturer's instructions. The pooled RNA libraries were
550 sequenced on an Illumina HiSeq2000 to obtain 100-bp paired-end reads. RNA-
551 sequencing reads were aligned to the human reference genome hg19 and quantified

552 using the stranded option of STAR version 2.4.2a30. Furthermore, the DESeq2
553 package was used to obtain normalized expression values as described[35]. The GSEA
554 desktop application was utilized for enrichment analysis of the indicated gene sets.
555 Gene set databases downloaded from the Broad Institute website or custom-derived
556 signatures were analyzed using default settings with 2000 permutations.
557
558 **Cell lines**
559 HMLE-Twist1-ER, generated as previously described[36,37], were kindly gifted by Robert
560 A. Weinberg (Whitehead Institute). HMLE-Twist1-ER ($CD24^{high}$) cells were cultured in
561 Mammary Epithelial Cell Basal Medium containing 0.004 ml/ml BPE, 10 ng/ml EGF, 5
562 µg/ml Insulin and 0.5 µg/ml hydrocortisone (PromoCell) supplemented with Pen/Strep
563 (Invitrogen) and Blasticidin S HCl (Thermo Fisher Scientific) at a final concentration of
564 10 µg/ml. To obtain HMLE-Twist1-ER $CD24^{high}$ single-cell clones (SCCs), cell were
565 seeded to a 96-well plate (0.3 cells/well). Wells were checked by eye for single-cells.
566 Wells with a single cell were further passaged and expanded. For Twist1-activation,
567 cells were treated with (Z)-4-Hydroxytamoxifen (TAM, Sigma-Aldrich) at a final
568 concentration of 20 nM for the indicated number of days. HMLE-Twist1-ER *ZEB1*
569 overexpression cells were isolated with cloning cylinders (Sigma) and propagated in
570 medium further supplemented with Puromycin Dihydrochloride (Thermo Fisher
571 Scientific) at a final concentration of 1 µg/ml. For tracing experiments, E-SCC cells
572 were lentivirally transduced with pRRL-cPPT-CMV-GFP-W and fluorescence-activated
573 cell sorting (FACS) was used to select GFP-positive cells. SUM-149PT cells were
574 cultivated in F12 containing 5% FBS. SUM-149PT cells were authenticated using
575 Multiplex Cell Authentication (Multiplexion, Heidelberg, Germany) as described[38]. The
576 SNP profiles matched known profiles or were unique. The purity of SUM-149PT cells
577 was validated using the Multiplex cell Contamination Test (Multiplexion, Heidelberg)

578 as described[39]. The medium of all cells was changed every two to three days.

579

580 **RNA isolation and qRT-PCR**

581 RNA was isolated using the miRNeasy Mini Kit (Qiagen) or the mRNeasy Mini Kit
582 (Qiagen). Reverse transcription of mRNA was performed with the EasyScriptPlus Kit.
583 For qRT-PCR, the Power SYBR Green-PCR Master Mix (Applied Biosystems) was
584 used. *RPL32* was used as a control for normalization. Reverse transcription of miRNAs
585 was performed with the miScript RT Kit (Qiagen) and qRT-PCR was performed with
586 the Power SYBR Green-PCR Master Mix (Applied Biosystems) and miScript Primer
587 Assays (control/normalization:HS-RNU6-2_11, *MIR141*:HS-miR-141_1,
588 *MIR200A*:HS-miR-200a_1, *MIR200B*:HS-miR-200b_3, *MIR200C*:HSmiR200c_1,
589 Qiagen). Samples ran on a QuantStudio 12K Flex qPCR system (Life Technologies).
590 Data were analysed with the ΔCt method and relative expression levels are displayed
591 as 1000 x $2^{-\Delta Ct}$. Following primer pairs were used:
592 *CDH1*: forward 5'-TGCCCAGAAAATGAAAAAGG-3' and reverse 5'-
593 GTGTATGTGGCAATGCGTTC-3', *EPCAM*: forward 5'-
594 ATAACCTGCTCTGAGCGAGTG-3' and reverse 5'-
595 TGCAGTCCGCAAACTTTTACTA-3', *FN1*: forward 5'-
596 CAGTGGGAGACCTCGAGAAG-3' and reverse 5'- TCCCTCGGAACATCAGAAAC-3',
597 *Twist1*: forward 5'-GGACAAGCTGAGCAAGATTCA-3' and reverse 5'-
598 CGGAGAAGGCGTAGCTGAG-3', *OVOL2*: forward 5'-
599 ACAGGCATTCGTCCCTACAAA-3' and reverse 5'- CGCTGCTTATAGGCATACTGC-
600 3', *RPL32*: forward 5'- CAGGGTTCGTAGAAGATTCAAGGG-3' and reverse 5-
601 'CTTGGAGGAAACATTGTGAGCGATC-3', *VIM*: forward 5'-
602 GAGAACTTTGCCGTTGAAGC-3' and reverse 5'- GCTTCCTGTAGGTGGCAATC-3',
603 *WNT5A*: forward 5'- ATGGCTGGAAGTGCAATGTCT-3' and reverse 5'-

604 ATACCTAGCGACCACCAAGAA-3', *ZEB1*: forward 5'-
605 GCACAAGAAGAGCCACAAGTAG-3' and reverse 5'-
606 GCAAGACAAGTTCAAGGGTTC-3'.
607
608 **Immunofluorescence**
609 Cells were cultured on coverslips coated with poly-D-lysine (Sigma-Aldrich), in floating
610 3D-collagen gels, or on murine lung slices. Cells were fixed with 4% paraformaldehyde
611 for 10 to 15 minutes and permeabilized with 0.2% Triton X-100. After blocking with
612 10% normal goat serum in 0.1% BSA (Sigma-Aldrich), coverslips, floating 3D-collagen
613 gels, and murine lung slices were incubated overnight with primary antibodies in 0.1%
614 BSA as follows: anti-CDH1 (clone EP700Y, Biozol, 1:250) or anti-CDH1-Alexa-488
615 (clone 24E10, New England Biolabs, 1:50), anti-Twist1 (clone Twist2C1a, Santa Cruz,
616 1:500), anti-VIM (clone V9, Abnova, 1:100). Secondary antibodies were coupled to
617 Alexa-488, -594, or -546 (Life Technologies, 1:250). Cell nuclei were visualized with
618 40,6-diamidino-2-phenylindole-dihydrochloride (DAPI, Sigma-Aldrich). Slides were
619 mounted with Aqua-Poly/Mount reagent (Polysciences). Corrected total cell
620 fluorescence (CTCF) of DAPI was calculated using the following formula: CTCF =
621 integrated density – (area of selected cells x mean fluorescence of background
622 readings). Pictures were taken with a Zeiss Axio Imager.M2 using Zen software or with
623 an Olympus Confocal using FV10-ASW software.
624
625 **Fluorescence-Activated Cell Sorting (FACS) and Flow Cytometry**
626 Metastatic breast cancer cells were stained in a 1% BSA solution containing 2 mM
627 Ethylenediaminetetraacetic acid (EDTA) under the presence of FcR blocking reagent
628 (Miltenyi). HMLE-Twist1-ER cell suspensions were stained in Mammary Epithelial Cell
629 Basal Medium (PromoCell). Propidium Iodide (PI), or 7-AAD (BD Biosciences, 1:125

630 were used to exclude dead cells, depending on the staining panel. Cells were sorted
631 and analysed on a FACSAria Illu, an LSR Fortessa, and a FACS Aria Fusion (all BD)
632 and further analysed with FlowJo. Antibodies: anti-EPCAM-FITC (VU-1D9 clone,
633 Biozol, 1:25, or REA764 clone, Miltenyi, 1:11), anti-CD45-VioBlue (REA747 clone,
634 Miltenyi, 1:11).
635
636 **Immunoblotting**
637 Adherent cells were harvested by scraping on ice after 1 wash with PBS. Collected cell
638 pellets were resuspended in RIPA buffer (50 mM Tris pH 8.0, 150 mM NaCl, 1% NP-
639 40, 0.5% sodium deoxycholate, 0.1% sodium dodecyl sulphate and 5 mM EDTA pH
640 8.0) containing a protease and a phosphatase inhibitor (Sigma-Aldrich). Protein
641 concentration was measured using the DC Protein Assay (Bio-Rad Laboratories).
642 10 µg protein were separated on 10% SDS-PAGE gels and transferred on PVDF
643 membranes by wet-blot transfer. Immunoblotting was performed using the following
644 primary antibodies: CDH1 (clone EP700Y, Biozol, 1:25000), ZEB1 (clone H-102, Santa
645 Cruz Biotechnology, 1:200) or ZEB1 (Sigma, 1:5000), ACTB (clone AC-15, Abcam,
646 1:6000) was used as a loading control. Secondary antibodies (anti-mouse and anti-
647 rabbit) were conjugated to horseradish peroxidase (Jackson Immuno Research,
648 1:12500). Chemiluminescence reaction was activated with ECL Prime Western
649 Blotting Detection Reagent (GE Healthcare) and detection was carried out on a
650 ChemiDoc Imaging System using Image Lab software (Bio-Rad Laboratories).
651
652 **Floating 3D-collagen gels**
653 Floating 3D-collagen gels with a final concentration of 1.3 mg/ml collagen I (collagen
654 type I from rat tail, Corning) were prepared as previously described[7,15]. Briefly, 300
655 HMLE-Twist1-ER cells were embedded per collagen gel. Cells were further cultivated

656 in Mammary Epithelial Cell Basal Medium containing 0.004 ml/ml BPE, 10 ng/ml EGF,
657 5 µg/ml Insulin and 0.5 µg/ml hydrocortisone (PromoCell) supplemented with
658 Pen/Strep (Invitrogen) and Blasticidin S HCl (Thermo Fisher Scientific) at a final
659 concentration of 10 µg/ml. Medium was changed every two to three days. After 10 days
660 in culture, floating 3D-collagen gels were fixed with 4% paraformaldehyde for 15
661 minutes. Immunofluorescent staining was performed as described above. To visualize
662 colonies, floating 3D-collagen gels were incubated in a carmine alum staining solution
663 (2 g/l carmine (Sigma-Aldrich), 5 g/l aluminium potassium sulphate (Sigma-Aldrich),
664 two crystals of thymol) at 4°C overnight. Pictures of gels were taken with a Leica
665 DFC450 C Stereomicroscope with a Plan 0.8x LWD objective and the Leica Application
666 Suite V4 software. Pictures were stitched with Panorama Stitcher. Carmine positive
667 colonies were counted using ImageJ.
668
669 **Colonizing assay on murine precision cut lung slices (PCLS)**
670 PCLS were generated as previously described[17]. Briefly, C57BL6/N mice of 8-12
671 weeks were intubated and after the dissection of the diaphragm, lungs were flushed
672 through the heart with sterile sodium chloride solution. Using a syringe pump, lungs
673 were filled with low gelling temperature agarose (2% by weight, A9414; Sigma; kept at
674 40°C) in sterile cultivation medium (DMEM/Ham's F12 (Gibco) supplemented with 100
675 U/ml penicillin, 100 µg/ml streptomycin and 2.5 µg/ml amphotericin B (Sigma)).
676 Separated lobes were cut with a vibratome (Hyrax V55; Zeiss, Jena, Germany) to a
677 thickness of 300 µm using a speed of 10–12 µm/s, a frequency of 80 Hz and an
678 amplitude of 1 mm. The PCLS were cultivated in sterile cultivation medium containing
679 0.1%FCS. HMLE-Twist1-ER cells were lentivirally transduced with pRRL-cPPT-CMV-
680 GFP-W. Fluorescence-activated cell sorting (FACS) was used to select GFP positive
681 cells. $2x10^5$ cells were plated per lung slice and cultured in Mammary Epithelial Cell

682 Basal Medium containing 0.004 ml/ml BPE, 10 ng/ml EGF, 5 µg/ml Insulin and 0.5
683 µg/ml hydrocortisone (PromoCell) supplemented with Pen/Strep (Invitrogen) for 5
684 days, changing the medium every day.
685
686 **CRISPR/Cas9 of *ZEB1***
687 We made use of the transient expression of Cas9 and four guide RNAs (gRNAs)
688 targeting two regions of exons that are found in all 9 transcript variants of *ZEB1*. Guide
689 RNAs (gRNAs) were designed with Benchling and the MIT CRISPR design tool
690 (http://crispr.mit.edu/). For creating a vector harbouring all four *ZEB1* gRNAs, gRNAs
691 were cloned by applying the string assembly gRNA cloning (STAgR) protocol[40]. For
692 Gibson Assembly, a Gibson Assembly Master Mix (New England Biolabs) was used
693 according to manufacturer's instructions. For transformation into XL10-Gold
694 ultracompetent cells (Agilent Technologies) the Gibson Assembly was diluted 1:4.
695 Purified plasmids were transfected into HMLE-Twist1-ER cells. In detail, 24h before
696 transfection, 1.5 – $2x10^5$ cells were seeded in 6-well dishes. Cells were then
697 transfected with a Cas9-GFP-expressing plasmid (pSpCas9(BB)-2A-GFP) and the
698 gRNA containing STAgR-Neo plasmid using the TransIT-X2 transfection reagent
699 (Mirus Bio LLC) according to manufacturer's instructions. As a control, cells were
700 transfected with the Cas9-GFP plasmid and a plasmid harbouring the guide RNA
701 scaffold and termination sequence. After 2.5 days cells were sorted for GFP
702 expression on a FACSAriaIIIu (BD Biosciences). To obtain single-cell clones, sorted
703 cells were seeded into 96-well plates (1 cell/well). Wells were checked by eye for
704 single-cells. Wells with a single-cell were further passaged and expanded. To screen
705 for cells with successful deletion, cells were lysed in DNAzol reagent (Thermo Fisher
706 Scientific) and genomic DNA (gDNA) of *ZEB1* knockout single-cell clones was isolated
707 with the DNAzol Reagent (Invitrogen) according to the manufacturer's instructions for

708 adherent cells (monolayer). PCRs of the specific loci were performed to screen for
709 DNA modifications and *ZEB1* knockout was validated by immunoblotting.
710 Following gRNAs were used: *ZEB1* NM128128 Exon 5: 5'-
711 GCCTCTATCACAATATGGAC-3' and 5'-ACAACTCAGCCCTCAATGGA-3', *ZEB1*
712 NM128128 Exon 7: 5'-AGTTCTGTCACAAGCATGCA-3' and 5'-
713 TTGCCGTATCTGTGGTCGTG-3'.
714 Following PCR primers were used: *ZEB1* NM128128 Exon 5: forward 5'-
715 GCATAGGGACTCAGTGGAAACT-3' and reverse 5'-
716 AGGAGGCAACTCCCTTTACTAC-3', *ZEB1* NM128128 Exon 7: forward 5'-
717 GGTCGGTGAAATGGGATAAGAAAAA-3' and reverse 5'-
718 ACCACCAGTGAAAACCCCATT-3'.
719
720 **Overexpression of *ZEB1***
721 To overexpress *ZEB1*, we made use of the All-in-One piggyBac system designed for
722 inducible transgene expression[41]. In detail, the *ZEB1* (NM1174096) cDNA was cloned
723 into the pENTR1A-no ccdb vector (#17398, Addgene) to generate the pENTR1A-*ZEB1*
724 vector. Next, the Gateway LR Clonase II Enzyme mix (Invitrogen) was used to transfer
725 the *ZEB1* cDNA from the pENTR1A-*ZEB1* vector into the PB-TAC-ERP2 (#80478,
726 Addgene) to generate the PB-*ZEB1* vector. Cells were transfected with the linearized
727 PB-ZEB1 plasmid and the pCMV-hyPBase vector (kind gift of Roland Rad, TU Munich)
728 in a ratio of 4:1, respectively, using the TransIT-X2 transfection reagent (Mirus Bio
729 LLC) according to manufacturer's instructions. For selection, cells were cultured in
730 medium containing 1 µg/ml Puromycin Dihydrochloride (Thermo Fisher Scientific) 48
731 hours after transfection. Next, single-cell colonies were isolated using cloning cylinders
732 (Sigma) and expanded for further analysis.

733 **RNA-sequencing of HMLE-Twist1-ER cells**

734 Library preparation was performed using the TruSeq Stranded Total RNA Library Prep
735 Kit with Ribo-Zero (Illumina). Briefly, total RNA was isolated using the miRNeasy Mini
736 Kit (Qiagen) and RNA integrity number (RIN) was determined with the Agilent 2100
737 BioAnalyzer (RNA 6000 Nano Kit, Agilent). For library preparation, 1 µg of RNA was
738 depleted for cytoplasmatic rRNAs, fragmented, and reverse transcribed with the Elute,
739 Prime, Fragment Mix. A-tailing, adaptor ligation, and library enrichment were
740 performed as described in the High Throughput protocol of the TruSeq RNA Sample
741 Prep Guide (Illumina). RNA libraries were assessed for quality and quantity with the
742 Agilent 2100 BioAnalyzer and the Quant-iT PicoGreen dsDNA Assay Kit (Life
743 Technologies). RNA libraries were sequenced as 150 bp paired-end runs on an
744 Illumina HiSeq4000 platform. The STAR aligner (v 2.4.2a) with modified parameter
745 settings (--twopassMode=Basic) is used for split-read alignment against the human
746 genome assembly hg19 (GRCh37) and UCSC knownGene annotation[42]. To quantify
747 the number of reads mapping to annotated genes we use HTseq-count (v0.6.0)[43].
748 FPKM (Fragments Per Kilobase of transcript per Million fragments mapped) values are
749 calculated using custom scripts. PCA plots were created with the R package ggplot2[44].
750

751 **Omni-ATAC-sequencing of HMLE-Twist1-ER cells**

752 ATAC-sequencing was done as described previously[45]. Briefly, 50,000 cells (viability
753 > 90%) were harvested by trypsinisation and pelleted (500 rcf, 4°C, 5 min). If the cell
754 viability of cell suspensions used for ATAC-seq was below 90%, dead cells were
755 removed with the Dead Cell Removal Kit (Milteny Biotech) according to the
756 manufacturer's instructions and then harvested as the others. Cell pellets were
757 resuspended in ATAC Resuspension Buffer (10mM Tris-HCl pH 7.4, 10 mM NaCl, 3
758 mM $MgCl_2$) supplemented with 0.1% NP40, 0.1% Tween-20 and 0.01% digitonin for

759 lysis, incubated on ice for 3 min and then 1 ml of ATAC Resuspension Buffer
760 supplemented only with 0.1% Tween-20 was added and spun (500 rcf, 4°C, 10 min) to
761 collect nuclei. Nuclei were subsequently re-suspended in 50 µl of Transposase
762 Reaction containing 25 µl 2x Tagmentation Buffer (20 mM Tris-HCl pH 7.6, 10 mM
763 $MgCl_2$, 20% dimethyl Formamide, $H_2O$), 2.5 µl Tn5 Transposase (Illumina Nextera
764 DNA Library Preparation Kit), 5.25 µl $H_2O$, 16.5 µl PBS, 0.25 µl of 2% digitonin
765 (Promega) and 0.5 µl of 10% Tween-20. Reactions were incubated for 30 min at 37°C
766 in a thermomixer shaking at 900 rpm and DNA was then purified using Qiagen PCR
767 clean-up MinElute kit (Qiagen). Transposed DNA was subsequently amplified in 50 µl
768 reactions with custom primers as described previously[46]. After 4 cycles amplification,
769 libraries were then monitored with qPCR: 5 µl PCR sample in a 15 µl reaction with the
770 same primers. qPCR output was monitored for the ΔRN; 0.25 ΔRN cycle number was
771 used to estimate the number of additional cycles of the PCR reaction needed for the
772 remaining PCR samples. Amplified libraries were purified with the Qiagen PCR clean-
773 up MinElute kit and size selected for fragments less than 600 bp using the Agencourt
774 AMPure XP beads (Beckman Coulter). Libraries were quality controlled by Qubit and
775 Agilent DNA Bioanalyzer analysis. Deep sequencing was performed on a HiSeq 1500
776 system according to the standard Illumina protocol for 50bp single-end reads. ATAC-
777 seq reads were aligned to the human genome hg38 using Bowtie[47] with options "-q -n
778 2 --best --chunkmbs 2000 -p 32 -S". ATAC peaks over Input background were
779 identified using Homer[48] findPeaks.pl with option "-style factor". Peaks from all samples
780 were merged using mergePeaks resulting in a unified Peak set. The peak list was
781 filtered for promoter-associated peaks (distance to TSS < 1000bp) with bedtools. Raw
782 ATAC coverage counts were then calculated with annotatePeaks. PCA analysis was
783 performed on ATAC peaks coverage data with the R function prcomp. The list of
784 differential ATAC peaks was determined with the DESeq2 results function for all

785 possible comparisons between the samples and filtered for adjusted p-value < 0.05
786 and log2 fold change > 3. The cluster heatmap was generated based on normalized
787 coverage data of all differential ATAC peaks using the R pheatmap package in
788 k_means mode with 12 clusters. Cluster-specific peaks were further analysed for
789 transcription factor motifs using homer findMotifsGenome function in *de novo* mode.
790

791 **Data presentation and statistical analyses**

792 Data are presented as mean±SEM of n=x experiments, with x indicating the number
793 of independent experiments performed, unless otherwise stated. Statistical analysis
794 was performed using GraphPad Prism software. In general, a p-value below 0.05 was
795 considered significant.
796

797 **Data availability**

798 The datasets that support the findings of this study have been deposited in the Gene
799 Expression Omnibus (GEO) under the accession code GSE138329.
800

801 **Acknowledgements**

802 We thank Christopher Breunig and Stefan Stricker (Helmholtz Center Munich) for
803 sharing reagents and guidance for STAgR cloning, and Robert Weinberg (Whitehead
804 Institute) for providing HMLE-Twist1-ER cells. We thank all members of the Scheel
805 group, especially Lisa Meixner and Elena Panzilius, for sharing experimental expertise.
806 We also thank Sandy Lösecke for technical assistance during RNA-sequencing. We
807 thank Steffen Schmitt, Klaus Hexel, Ann Atzberger, and Marcus Eich from the DKFZ
808 Flow Cytometry Core Facility for their kind assistance and all members of the DKFZ
809 Laboratory Animal Core Facility for excellent animal welfare and husbandry. We are
810 grateful to Roland Rad (Technical University Munich) for providing the hyperactive

transposase for the PiggyBac assay. We further thank Heiko Lickert (Helmholtz Center Munich), Maximilian Reichert (Technical University Munich), Thordur Oskarsson, and Michael Milsom (HI-STEM Heidelberg) for constructive discussions and Nina Cabezas-Wallscheid (Max Planck Institute Freiburg) for her support. Finally, we thank Nicola Aceto (University of Basel) for helpful discussions and for his support. The work in the G.S. lab is funded by Deutsche Forschungsgemeinschaft (SFB1064 - A11 and SFB1321 - P13). This work was further supported by the Transluminal-B and Integrate-TN consortia funded by the Deutsche Krebshilfe, the Swiss-Bridge Award and the Dietmar Hopp Foundation (all to A.T.) and by a Max Eder Grant of the German Cancer Aid Foundation (Deutsche Krebshilfe 110225 to C.H.S.).

**Author Contributions**

M.S., L.E., M.R.S., A.T., and C.H.S. conceived the project and designed experiments. L.E., M.S., H.D.M., C.K., J.M.B., M.R., V.V., S.H., and R.W. performed research and analysed the data. M.F., E.E., R.W., E.D., and S.H. analysed the data, provided crucial datasets and contributed to data interpretation. H.D.M. and G.S. performed ATAC-sequencing and data analysis. E.G. and T-M.S. performed RNA-sequencing. T.S. performed RNA-sequencing data analysis. M.L. and M.K. provided lung slices and the according assay. A.S., M.Sü., and S.S. provided patient samples, supervised and managed clinical data. N.P. and W.W. performed next-generation sequencing of mutational hotspots and supervised histopathological analysis of patient-derived xenografts. L.E. and M.S. assembled the figures. L.E., M.S., A.T. and C.H.S. wrote the manuscript. All authors read and approved the manuscript.

**Competing interests**

The authors declare no competing interests.

837 **References**


838 1. Howlader, N. *et al.* SEER Cancer Statistics Review, 1975-2016, National Cancer
839 Institute. Bethesda, MD, https://seer.cancer.gov/csr/1975_2016/, based on
840 November 2018 SEER data submission, posted to the SEER web site, April
841 2019. (2019).

842 2. Baccelli, I. *et al.* Identification of a population of blood circulating tumor cells from
843 breast cancer patients that initiates metastasis in a xenograft assay. *Nat.*
844 *Biotechnol.* **31**, 539–544 (2013).

845 3. Yu, M. *et al.* Circulating Breast Tumor Cells Exhibit Dynamic Changes in
846 Epithelial and Mesenchymal Composition. *Science (80-. ).* **339**, 580–584 (2013).

847 4. Tsai, J. H., Donaher, J. L., Murphy, D. A., Chau, S. & Yang, J. Spatiotemporal
848 Regulation of Epithelial-Mesenchymal Transition Is Essential for Squamous Cell
849 Carcinoma Metastasis. *Cancer Cell* **22**, 725–736 (2012).

850 5. Krebs, A. M. *et al.* The EMT-activator Zeb1 is a key factor for cell plasticity and
851 promotes metastasis in pancreatic cancer. *Nat. Cell Biol.* **19**, 518–529 (2017).

852 6. Ocaña, O. H. *et al.* Metastatic Colonization Requires the Repression of the
853 Epithelial-Mesenchymal Transition Inducer Prrx1. *Cancer Cell* **22**, 709–724
854 (2012).

855 7. Schmidt, J. M. *et al.* Stem-cell-like properties and epithelial plasticity arise as
856 stable traits after transient twist1 activation. *Cell Rep.* **10**, 131–139 (2015).

857 8. Kowalski, P. J., Rubin, M. a & Kleer, C. G. E-cadherin expression in primary
858 carcinomas of the breast and its distant metastases. *Breast Cancer Res.* **5**,
859 R217-22 (2003).

860 9. Fischer, K. R. *et al.* Epithelial-to-mesenchymal transition is not required for lung
861 metastasis but contributes to chemoresistance. *Nature* **527**, 472–476 (2015).

862 10. Zheng, X. *et al.* Epithelial-to-mesenchymal transition is dispensable for

863 metastasis but induces chemoresistance in pancreatic cancer. *Nature* **527**, 525–
864 530 (2015).
865 11. Pastushenko, I. *et al.* Identification of the tumour transition states occurring
866 during EMT. *Nature* **556**, 463–468 (2018).
867 12. Yu, M. *et al.* Circulating Breast Tumor Cells and Mesenchymal Composition.
868 **339**, (2019).
869 13. Casas, E. *et al.* Snail2 is an essential mediator of twist1-induced epithelial
870 mesenchymal transition and metastasis. *Cancer Res.* **71**, 245–254 (2011).
871 14. Scheel, C. & Weinberg, R. A. Cancer stem cells and epithelial-mesenchymal
872 transition: Concepts and molecular links. *Semin. Cancer Biol.* **22**, 396–403
873 (2012).
874 15. Linnemann, J. R. *et al.* Quantification of regenerative potential in primary human
875 mammary epithelial cells. *Development* **142**, 3239–3251 (2015).
876 16. Shi, J. *et al.* Disrupting the Interaction of BRD4 with Diacetylated Twist
877 Suppresses Tumorigenesis in Basal-like Breast Cancer. *Cancer Cell* **25**, 210–
878 225 (2014).
879 17. Uhl, F. E. *et al.* Preclinical validation and imaging of Wnt-induced repair in human
880 3D lung tissue cultures. *Eur. Respir. J.* **46**, 1150–1166 (2015).
881 18. Kotlyar, M. *et al.* In silico prediction of physical protein interactions and
882 characterization of interactome orphans. *Nat. Methods* **12**, 79–84 (2014).
883 19. Huttlin, E. L. *et al.* Architecture of the human interactome defines protein
884 communities and disease networks. *Nature* **545**, 505–509 (2017).
885 20. Sánchez-Tilló, E. *et al.* ZEB1 represses E-cadherin and induces an EMT by
886 recruiting the SWI/SNF chromatin-remodeling protein BRG1. *Oncogene* **29**,
887 3490–3500 (2010).
888 21. Vannier, C., Mock, K., Brabletz, T. & Driever, W. Zeb1 regulates E-cadherin and

889 Epcam (epithelial cell adhesion molecule) expression to control cell behavior in
890 early zebrafish development. *J. Biol. Chem.* **288**, 18643–18659 (2013).
891 22. Jacobs, J. *et al.* The transcription factor Grainy head primes epithelial enhancers
892 for spatiotemporal activation by displacing nucleosomes. *Nat. Genet.* **50**, 1011–
893 1020 (2018).
894 23. Werner, S. *et al.* Dual roles of the transcription factor grainyhead-like 2 (GRHL2)
895 in breast cancer. *J. Biol. Chem.* **288**, 22993–23008 (2013).
896 24. Chen, A. F. *et al.* GRHL2-Dependent Enhancer Switching Maintains a
897 Pluripotent Stem Cell Transcriptional Subnetwork after Exit from Naive
898 Pluripotency. *Cell Stem Cell* **23**, 226-238.e4 (2018).
899 25. Hong, T. *et al.* An Ovol2-Zeb1 Mutual Inhibitory Circuit Governs Bidirectional and
900 Multi-step Transition between Epithelial and Mesenchymal States. *PLoS*
901 *Comput. Biol.* **11**, 1–20 (2015).
902 26. Brabletz, S. & Brabletz, T. The ZEB/miR-200 feedback loop--a motor of cellular
903 plasticity in development and cancer? *EMBO Rep.* **11**, 670–677 (2010).
904 27. Padmanaban, V. *et al.* E-cadherin is required for metastasis in multiple models
905 of breast cancer. *Nature* **573**, 439–444 (2019).
906 28. Kröger, C. *et al.* Acquisition of a hybrid E/M state is essential for tumorigenicity
907 of basal breast cancer cells. *Proc. Natl. Acad. Sci. U. S. A.* **116**, 7353–7362
908 (2019).
909 29. Celià-Terrassa, T. *et al.* Epithelial-mesenchymal transition can suppress major
910 attributes of human epithelial tumor-initiating cells. **122**, (2012).
911 30. Gomis, R. R., Alarcón, C., Nadal, C., Van Poznak, C. & Massagué, J. C/EBPβ
912 at the core of the TGFβ cytostatic response and its evasion in metastatic breast
913 cancer cells. *Cancer Cell* **10**, 203–214 (2006).
914 31. Noll, E. M. *et al.* CYP3A5 mediates basal and acquired therapy resistance in

915 different subtypes of pancreatic ductal adenocarcinoma. *Nat. Med.* **22**, 278–287
916 (2016).
917 32. Pfarr, N. *et al.* Targeted next-generation sequencing enables reliable detection
918 of HER2 (ERBB2) status in breast cancer and provides ancillary information of
919 clinical relevance. *Genes, Chromosom. Cancer* **56**, 255–265 (2017).
920 33. Kriegsmann, M. *et al.* Mutational profiles in triple-negative breast cancer defined
921 by ultradeep multigene sequencing show high rates of PI3K pathway alterations
922 and clinically relevant entity subgroup specific differences. *Oncotarget* **5**, (2014).
923 34. Konukiewitz, B. *et al.* Pancreatic neuroendocrine carcinomas reveal a closer
924 relationship to ductal adenocarcinomas than to neuroendocrine tumors G3.
925 *Hum. Pathol.* **77**, 70–79 (2018).
926 35. Raffel, S. *et al.* BCAT1 restricts αkG levels in AML stem cells leading to IDHmut-
927 like DNA hypermethylation. *Nature* **551**, 384–388 (2017).
928 36. Mani, S. A. *et al.* The Epithelial-Mesenchymal Transition Generates Cells with
929 Properties of Stem Cells. *Cell* **133**, 704–715 (2008).
930 37. Yang, J. *et al.* Twist, a Master Regulator of Morphogenesis , Plays an Essential
931 Role in Tumor Metastasis. *Cell* **117**, 927–939 (2004).
932 38. Castro, F. *et al.* High-throughput SNP-based authentication of human cell lines.
933 *Int. J. Cancer* **132**, 308–314 (2013).
934 39. Schmitt, M. & Pawlita, M. High-throughput detection and multiplex identification
935 of cell contaminations. *Nucleic Acids Res.* **37**, (2009).
936 40. Breunig, C. T. *et al.* One step generation of customizable gRNA vectors for
937 multiplex CRISPR approaches through string assembly gRNA cloning (STAgR).
938 *PLoS One* **13**, 1–12 (2018).
939 41. Kim, S.-I. *et al.* Inducible Transgene Expression in Human iPS Cells Using
940 Versatile All-in-One piggyBac Transposons. in *Induced Pluripotent Stem (iPS)*

941 *Cells* 111–131 (2015). doi:10.1007/7651_2015_251

942 42. Dobin, A. *et al.* STAR: Ultrafast universal RNA-seq aligner. *Bioinformatics* **29**,
943 15–21 (2013).

944 43. Anders, S., Pyl, P. T. & Huber, W. HTSeq-A Python framework to work with high-
945 throughput sequencing data. *Bioinformatics* **31**, 166–169 (2015).

946 44. Wickham, H. *ggplot2*. (Springer International Publishing, 2016).
947 doi:10.1007/978-3-319-24277-4

948 45. Corces, M. R. *et al.* An improved ATAC-seq protocol reduces background and
949 enables interrogation of frozen tissues. *Nat. Methods* **14**, 959–962 (2017).

950 46. Buenrostro, J. D., Giresi, P. G., Zaba, L. C., Chang, H. Y. & Greenleaf, W. J.
951 Transposition of native chromatin for fast and sensitive epigenomic profiling of
952 open chromatin, DNA-binding proteins and nucleosome position. *Nat. Methods*
953 **10**, 1213–1218 (2013).

954 47. Langmead, B. Aligning Short Sequencing Reads with Bowtie. *Curr. Protoc.*
955 *Bioinforma.* **32**, 11.7.1-11.7.14 (2010).

956 48. Heinz, S. *et al.* Simple combinations of lineage-determining transcription factors
957 prime cis-regulatory elements required for macrophage and B cell identities. *Mol.*
958 *Cell* **38**, 576–89 (2010).

959 **Figure legends**

960 **Figure 1: High EPCAM expression correlates with disease-propagating potential**
961 **in metastatic breast cancer cells**

962 **a,** FACS plot of CD45 and EPCAM of cells from liquid biopsies. Gates used for sorting
963 cells with different EPCAM levels are highlighted. TNBC, Triple Negative Breast
964 Cancer; Pat., Patient. **b,** Number of mice with tumours formed by cells injected into the
965 mammary fat pad in limiting dilution. The number of mice injected (n=x) is indicated at
966 the centre of each chart. The table shows numbers of mice with orthotopic tumour
967 growth (tumour) and no orthotopic tumour growth (no tumour), the calculated TIC
968 frequency of tumour-initiating cells (TIC), and the number of mice with lung
969 metastases. Chi-square test; p-value: ∗∗∗∗<0.0001. ER, oestrogen receptor. **c,** Allelic
970 frequency values in sorted $CD45^{+}$, $EPCAM^{neg}$ (neg), $EPCAM^{low}$ (low), and $EPCAM^{high}$
971 (high) cell subsets presented as a single percentage value per mutation per patient.
972 Mutations are ordered as bars from left to right as they are listed in the table below.
973 n=7; Wilcoxon matched-pairs signed rank test; p-values: ∗=0.039, ∗∗=0.0098, ns=not
974 significant. **d,** Hallmark gene set enrichment analysis of RNA-sequencing data of
975 sorted $EPCAM^{high}$ and $EPCAM^{low}$ cells from an $ER^{+}$ and an $ER^{-}$ patient. Signatures
976 with FDR<0.25 are ranked by the % of core-enrichment. Signature size indicates the
977 overall number of genes composing the reference signature. n=4.

978

979 **Figure 2: A subset of HMLE-Twist1-ER cells maintains EPCAM expression**
980 **during EMT-induction**

981 **a,** FACS plot of EPCAM of HMLE-Twist1-ER bulk cells untreated (-TAM) or treated
982 with Tamoxifen for 21 days (+TAM 21d). The gates used for cell sorting are highlighted.
983 **b,** Flow cytometric staining of EPCAM of sorted $EPCAM^{neg}$ and $EPCAM^{pos}$ cells after
984 10 days of Tamoxifen withdrawal (+TAM21d/-TAM10d). Gates for EPCAM were set

985 according to unstained control as indicated by cells only stained for 7AAD (7AAD ctrl).
986 **c,** log relative mRNA expression levels of *EPCAM*, *CDH1*, *OVOL2*, and *ZEB1* of sorted
987 $EPCAM^{neg}$ (neg) and $EPCAM^{pos}$ (pos) HMLE-Twist1-ER cells treated as described in
988 b. n=2; mean ± SEM; multiple t-tests (Holm-Sidak correction); p-values: ∗<0.05,
989 ∗∗<0.005. **d,** Immunofluorescence staining of DAPI (blue), E-cadherin (CDH1, green),
990 and Vimentin (VIM, red) of organoids formed by sorted $EPCAM^{pos}$ HMLE-Twist1-ER
991 cells in floating 3D-collagen gels treated as described in b. Scale bar: 50 µm. Positive
992 control for Vimentin not shown. **e,** Number of carmine positive-stained colonies per gel
993 of sorted $EPCAM^{neg}$ (neg) and $EPCAM^{pos}$ (pos) HMLE-Twist1-ER cells in floating 3D-
994 collagen gels treated as described in b. n=2; mean ± SEM.
995
996 **Figure 3: A subset of breast cancer single-cell clones resists complete EMT and**
997 **maintains the ability to proliferate in different environments**
998 **a,** Bright field images of a representative E-SCC (E1) and a representative M-SCC
999 (M2), untreated (-TAM), treated with Tamoxifen for 7 days (+TAM 7d), or treated with
1000 Tamoxifen for 14 days (+TAM 14d). Scale bar: 100 µm. **b,** Immunofluorescence
1001 staining of DAPI (blue), E-cadherin (CDH1, green), and Vimentin (VIM, red) of a
1002 representative E-SCC (E1) and a representative M-SCC (M2), untreated (-TAM),
1003 treated with Tamoxifen for 15 days (+TAM), or treated with Tamoxifen for 15 days
1004 followed by Tamoxifen withdrawal for 9 days (+/-TAM). Scale bar: 20 µm. **c,** Flow
1005 cytometric staining of EPCAM of a representative E-SCC (E1) and a representative M-
1006 SCC (M2), untreated (-TAM) or treated with Tamoxifen for 14 days (+TAM 14d). Gates
1007 for EPCAM were set according to a control as indicated by control cells only stained
1008 for 7AAD (7AAD ctrl). **d,** log relative mRNA expression levels of *EPCAM*, *CDH1*, *VIM*,
1009 and *FN1* in E-SCCs (E1-E3) and M-SCCs (M1-M3), treated as described in a. n=3;
1010 mean ± SEM; multiple t-tests (Holm-Sidak correction); p-values: ∗<0.05, ∗∗<0.005,

1011 ∗∗∗<0.0005, ns=not significant. **e,** Immunoblot of E-cadherin (CDH1), Vimentin (VIM),
1012 and β-actin (ACTB) of E-SCCs (E1-E3) and M-SCCs (M1-M3), treated as described in
1013 a. **f,** Immunofluorescence staining of DAPI (blue), E-cadherin (CDH1, green), and
1014 Vimentin (VIM, red) of E-SCCs (E1-E3) and M-SCCs (M1-M3), untreated (-TAM) or
1015 after 14 days of Tamoxifen treatment followed by Tamoxifen withdrawal for 7 days
1016 (+14d/-7d) growing in floating 3D-collagen gels. **g,** Number of carmine positive stained
1017 colonies per gel of E-SCCs and M-SCCs treated as described in f. n=3; mean ± SEM;
1018 multiple t-tests (Holm-Sidak correction); p-values: ∗∗=0.002, ns=not significant.
1019 **h,** Immunofluorescence staining of DAPI (blue) of $GFP^{pos}$ E-SCC (E) cells (green) and
1020 of DAPI (blue) and Vimentin (VIM, green) of M-SCC (M) cells growing on PCLS,
1021 untreated (-TAM) or after 14 days of Tamoxifen treatment followed by 5 days of
1022 Tamoxifen withdrawal (+/-TAM). Scale bar: 50 µm. **i,** log CTCF of DAPI intensity of
1023 representative images of $GFP^{pos}$ E-SCC (E) cells and M-SCC (M) cells growing on
1024 PCLS treated as described in h. n=4; mean ± SEM; multiple t-tests (Holm-Sidak
1025 correction); p-values: ∗∗=0.0022, ∗∗∗=0.0001. CTCF, Corrected Total Cell
1026 Fluorescence. **j,** Flow cytometric staining of EPCAM of SUM-149PT bulk cells. **k,** Flow
1027 cytometric staining of EPCAM of unsorted bulk, sorted $EPCAM^{neg}$, and $EPCAM^{pos}$
1028 SUM-149PT cells. **l,** Bioluminescence imaging of NSG mice after intra-femoral
1029 injection of an equal number (10,000) of $EPCAM^{neg}$ (neg) and $EPCAM^{pos}$ (pos)
1030 luciferase-labelled SUM-149PT cells showing fold-change to baseline signal at the
1031 termination of the experiment (20 weeks post-injection). The image shows two
1032 representative mice measured 10 weeks post-injection. The colour scale indicates the
1033 radiance of photons/sec/$cm^2$/sr. n=6; mean ± SEM; unpaired student's t-test with
1034 Welch's correction; p-value: ∗∗∗∗<0.0001. BLI, bioluminescence intensity.

1035 **Figure 4: EMT-induction causes genome-wide chromatin and transcriptional**
1036 **changes**

1037 **a,** Principal component (PC) analysis of ATAC-sequencing data of E-SCCs (△) and
1038 M-SCCs (○), untreated (-TAM), treated with Tamoxifen for 7 days (+TAM 7d), treated
1039 with Tamoxifen for 14 days (+TAM 14d), or treated with Tamoxifen for 14 days followed
1040 by Tamoxifen withdrawal for 7 days (+TAM 14d/-TAM 7d). Each data point represents
1041 one SCC at the indicated time point. **b,** Genome browser high resolution screenshot
1042 of ATAC-sequencing data of *EPCAM* and *CDH1* of one representative E-SCC (E) and
1043 one representative M-SCC (M), untreated (-TAM), treated with Tamoxifen for 7 days
1044 (+7d), or treated with Tamoxifen for 14 days (+14d). **c,** Heatmap of chromatin
1045 accessibility of 12 clusters of ATAC-sequencing peaks of E-SCCs and M-SCCs treated
1046 as described in b. **d,** Top 5 hits of Homer *de novo* transcription factor motif analysis of
1047 grouped clusters closing exclusively in M-SCCs (M) during Tamoxifen treatment
1048 (+TAM).

1049

1050 **Figure 5: The EMT-transcription factor ZEB1 is required for EMT, but not**
1051 **sufficient to overcome EMT-resistance**

1052 **a,** Heatmap of mean FPKM values of RNA-sequencing data of *GRHL1-3* of 3 E-SCCs
1053 (E) and 3 M-SCCs (M), untreated (-TAM), treated with Tamoxifen for 7 days (+7d), or
1054 treated with Tamoxifen for 14 days (+14d). **b,** Heatmap of mean FPKM values of RNA-
1055 sequencing data of *ZEB1-2* of 3 E-SCCs (E) and 3 M-SCCs (M), treated as described
1056 in a. **c,** log relative mRNA expression levels of *ZEB1* and *OVOL2* in E-SCCs (E1-E3)
1057 and M-SCCs (M1-M3), treated as described in a. n=3; mean ± SEM; multiple t-tests
1058 (Holm-Sidak correction); p-values: ∗<0.05, ∗∗<0.005, ns=not significant.
1059 **d,** Immunoblot of ZEB1 and β-actin (ACTB) of E-SCCs (E1-E3) and M-SCCs (M1-M3),
1060 treated as described in a. **e,** log relative mRNA expression levels of *ZEB1*, *CDH1*, and

1061 *OVOL2* of a M-SCC control clone and M-SCC *ZEB1* knockout clones (*ZEB1* KO #1-
1062 5), untreated (-TAM) or treated with Tamoxifen for 14 days (+TAM 14d). n=2; mean ±
1063 SEM. **f,** Immunoblot of ZEB1, E-cadherin (CDH1), and β-actin (ACTB) of a M-SCC
1064 control clone and M-SCC *ZEB1* knockout clones (*ZEB1* KO #1-5) treated as described
1065 in e. **g,** log relative mRNA expression levels of *ZEB1*, *CDH1*, and *OVOL2* of an E-SCC
1066 control clone and E-SCC *ZEB1* overexpression clones (*ZEB1* OE #1, #2) treated with
1067 DMSO or with 10 ng/ml, 100 ng/ml, or 1 µg/ml doxycycline (dox) for 7 days (+7d), or
1068 after 7 days of treatment followed by 14 days of withdrawal (+7d/-14d). n=3 technical
1069 replicates; mean ± SEM. **h,** Flow cytometric staining of EPCAM of an E-SCC control
1070 clone and E-SCC *ZEB1* overexpression clones (*ZEB1* OE #1, #2) treated with DMSO
1071 or with 1 µg/ml doxycycline (dox) for 7 days (7d).
1072
1073 **Figure 6: Maintenance of epithelial features promotes metastatic outgrowth**
1074 **a,** High EPCAM expression of metastatic breast cancer cells derived from pleural
1075 effusions of stage IV breast cancer patients enriches for tumour initiation and
1076 progression ($EPCAM^{high}$). On the contrary, reduced EPCAM levels of metastatic breast
1077 cancer cells prevent tumour initiation and progression and correlate with EMT
1078 ($EPCAM^{low}$). **b,** Upon Twist1-activation of HMLE-Twist1-ER cells, a subset of cells
1079 expresses high levels of ZEB1, represses the expression of epithelial genes, and
1080 undergoes stable and irreversible EMT, leading to loss of colonizing capacity in a
1081 three-dimensional environment ($EPCAM^{neg}$/M-SCCs). Knockout (KO) of ZEB1 in these
1082 cells inhibits trans-differentiation into a mesenchymal phenotype upon an EMT-
1083 stimulus. Another subset of cells expresses low levels of ZEB1 and resists repression
1084 of epithelial genes, resulting in resistance to EMT and maintenance of the colonizing
1085 capacity ($EPCAM^{pos}$/E-SCCs). Transient overexpression (OE) of ZEB1 within these

1086 cells activates EMT temporarily, but does not allow stable and irreversible trans-
1087 differentiation to a mesenchymal state.
1088
1089 **Supplementary Figure 1: High EPCAM expression correlates with disease-**
1090 **propagating potential in metastatic breast cancer cells**
1091 **a,** Table showing tumour stage, oestrogen receptor (ER) status, clinical subtype,
1092 histology type, and TNM classification of clinical patients #1-10. **b,** Gating strategy for
1093 patient-derived metastatic breast cancer cells. TNBC, Triple Negative Breast Cancer;
1094 Pat., Patient. **c,** Immunohistochemical staining of oestrogen receptor (ER),
1095 progesterone receptor (PR), E-cadherin (CDH1), Ki67, and Vimentin (VIM) of tumour
1096 sections from engrafted mammary fat pads. The xenografts originate from cells of
1097 patients with the indicated breast cancer subtype. Scale bar: 25 µm. TNBC, Triple
1098 Negative Breast Cancer; Pat., Patient. **d,** Immunohistochemical staining of oestrogen
1099 receptor (ER) and Ki67 of spontaneous lung metastases originating from $EPCAM^{high}$
1100 cells of patients with the indicated breast cancer subtype. Scale bar: 25 µm. TNBC,
1101 Triple Negative Breast Cancer; Pat., Patient. **e,** Gene set enrichment analysis (GSEA)
1102 plot of the growth-arresting response to TGF-β of $EPCAM^{high}$ versus $EPCAM^{low}$ cells
1103 from an $ER^{+}$ and an $ER^{-}$ patient. NES, normalized enrichment score; FDR, false
1104 discovery rate; P-VAL, p-value. **f,** GSEA plot of the META-PCNA proliferative signature
1105 of $EPCAM^{high}$ versus $EPCAM^{low}$ cells from an $ER^{+}$ and an $ER^{-}$ patient. NES,
1106 normalized enrichment score; FDR, false discovery rate; P-VAL, p-value.
1107
1108 **Supplementary Figure 2: A subset of HMLE-Twist1-ER cells maintains EPCAM**
1109 **expression during EMT-induction**
1110 **a,** Bright field pictures of HMLE-Twist1-ER cells, untreated (-TAM) or treated with
1111 Tamoxifen for 21 days (+TAM 21d). Scale bar: 100 µm. **b,** Bright field pictures of sorted

1112 EPCAM$^{neg}$ and EPCAM$^{pos}$ HMLE-Twist1-ER cells after 10 days of Tamoxifen
1113 withdrawal (+TAM21d/-TAM10d). Scale bar: 100 µm. **c,** Gating strategy for HMLE-
1114 Twist1-ER cells.
1115
1116 **Supplementary Figure 3: A subset of breast cancer single-cell clones resists**
1117 **complete EMT and maintains the ability to proliferate in different environments**
1118 **a,** Table showing number of epithelial (E-SCCs) and mesenchymal (M-SCCs) single-
1119 cell clones isolated from the HMLE-Twist1-ER bulk population and determined during
1120 Tamoxifen treatment. **b,** Immunofluorescence staining of DAPI (blue) and Twist1 (red)
1121 of E-SCCs (E1-E3) and M-SCCs (M1-M3), untreated (-TAM) or treated with Tamoxifen
1122 for 3 days (+TAM 3d), Scale bar: 20 µm. **c,** Immunoblot of Twist1 and β-actin (ACTB)
1123 of untreated E-SCCs and M-SCCs. Twist1 protein levels were quantified relatively to
1124 β-actin. **d,** log relative mRNA expression levels of *Twist1* and *WNT5A* in E-SCCs (E1-
1125 E3) and M-SCCs (M1-M3), untreated (-TAM), treated with Tamoxifen for 7 days (+TAM
1126 7d), or treated with Tamoxifen for 14 days (+TAM 14d). n=3; mean ± SEM. **e,** Bright
1127 field images of a representative E-SCC (E1) and a representative M-SCC (M2), treated
1128 with Tamoxifen for 14 days followed by Tamoxifen withdrawal for 7 days (+14d/-7d),
1129 14 days (+14d/-14d), or 21 days (+14d/-21d). Scale bar: 100 µm. **f,** log relative mRNA
1130 expression levels of *CDH1*, *VIM*, *FN1*, *OVOL2*, and *ZEB1* in E-SCCs (E1-E3) and M-
1131 SCCs (M1-M3), treated as described in e. n=3; mean ± SEM; multiple t-tests (Holm-
1132 Sidak correction); p-values: ∗<0.05, ∗∗<0.005, ∗∗∗<0.0005, ns=not significant.
1133 **g,** Bright field images of a representative E-SCC (E1) and a representative M-SCC
1134 (M2), treated with Tamoxifen for 21 days (+TAM 21d) or for 28 days (+TAM 28d). Scale
1135 bar: 100 µm. **h,** log relative mRNA expression levels of *CDH1*, *OVOL2*, and *ZEB1* in
1136 E-SCCs (E1-E3) and M-SCCs (M1-M3), treated as described in g. n=3; mean ± SEM;
1137 multiple t-tests (Holm-Sidak correction); p-values: ∗∗<0.005, ns=not significant.

1138 **Supplementary Figure 4: EMT-induction causes genome-wide chromatin and**
1139 **transcriptional changes**

1140 **a,** Principal component (PC) analysis of RNA-sequencing data of E-SCCs (△) and M-
1141 SCCs (○), untreated (-TAM), treated with Tamoxifen for 7 days (+TAM 7d), treated
1142 with Tamoxifen for 14 days (+TAM 14d), or treated with Tamoxifen for 14 days followed
1143 by Tamoxifen withdrawal for 7 days (+TAM 14d/-TAM 7d). Each data point represents
1144 one SCC at the indicated time point. **b,** Top 5 hits of Homer *known motif* (upper table)
1145 or *de novo* (two lower tables) transcription factor motif analysis of grouped clusters
1146 opening in M-SCCs (M) and E-SCCs (E, two upper tables) or opening exclusively in
1147 M-SCCs (M, lower table) during Tamoxifen treatment (+TAM).

1148

1149 **Supplementary Figure 5: The EMT-transcription factor ZEB1 is required for EMT,**
1150 **but not sufficient to overcome EMT-resistance**

1151 **a,** log relative mRNA expression levels of *MIR141 and MIR200A-C* in E-SCCs (E1-E3)
1152 and M-SCCs (M1-M3), untreated (-TAM), treated with Tamoxifen for 7 days (+TAM
1153 7d), or treated with Tamoxifen for 14 days (+TAM 14d). n=3; mean ± SEM; multiple t-
1154 tests (Holm-Sidak correction); p-values: ∗<0.05, ∗∗<0.005, ∗∗∗<0.0005, ns=not
1155 significant. **b,** Schematic illustration of the localisation of guide RNAs (gRNAs) for
1156 CRISPR/Cas9 of the *ZEB1* (NM00128128) gene. **c,** PCR products of targeted DNA
1157 regions of a M-SCC control clone and M-SCC *ZEB1* knockout clones (*ZEB1* KO #1-
1158 5). **d,** Bright field pictures of an M-SCC control clone and a representative M-SCC
1159 *ZEB1* knockout clone (*ZEB1* KO #1), untreated (-TAM) or treated with Tamoxifen for
1160 14 days (+TAM 14d). Scale bar: 100 µm. **e,** Bright field pictures of an E-SCC control
1161 clone and a representative E-SCC *ZEB1* overexpression clone (*ZEB1* OE #1), treated
1162 with DMSO or with 10 ng/ml, 100 ng/ml, or 1 µg/ml doxycycline (dox) for 7 days (+7d)

1163 or treated for 7 days followed by 14 days of withdrawal (+7d/-14d). Scale bar: 100 μm.

1164 **f,** Gating strategy for HMLE-Twist1-ER *ZEB1* overexpression and control cells.

**Figure 1: High EPCAM expression correlates with disease-propagating potential in metastatic breast cancer cells**

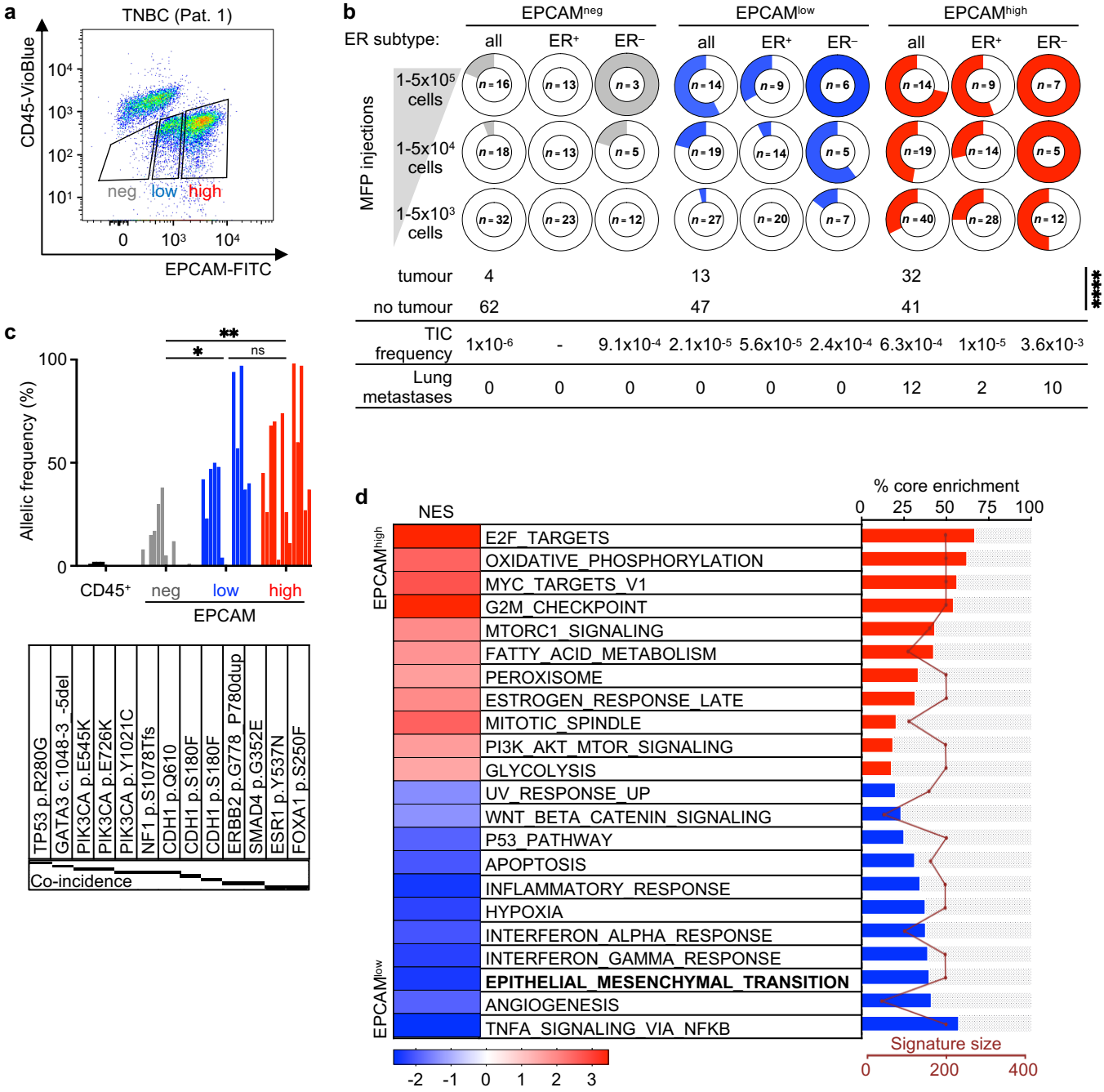


| | EPCAMneg all | EPCAMneg ER+ | EPCAMneg ER− | EPCAMlow all | EPCAMlow ER+ | EPCAMlow ER− | EPCAMhigh all | EPCAMhigh ER+ | EPCAMhigh ER− |
|---|---|---|---|---|---|---|---|---|---|
| tumour | 4 | | | 13 | | | 32 | | |
| no tumour | 62 | | | 47 | | | 41 | | |
| TIC frequency | $1x10^{-6}$ | - | $9.1x10^{-4}$ | $2.1x10^{-5}$ | $5.6x10^{-5}$ | $2.4x10^{-4}$ | $6.3x10^{-4}$ | $1x10^{-5}$ | $3.6x10^{-3}$ |
| Lung metastases | 0 | 0 | 0 | 0 | 0 | 0 | 12 | 2 | 10 |

**Figure 2: A subset of HMLE-Twist1-ER cells maintains EPCAM expression during EMT-induction**

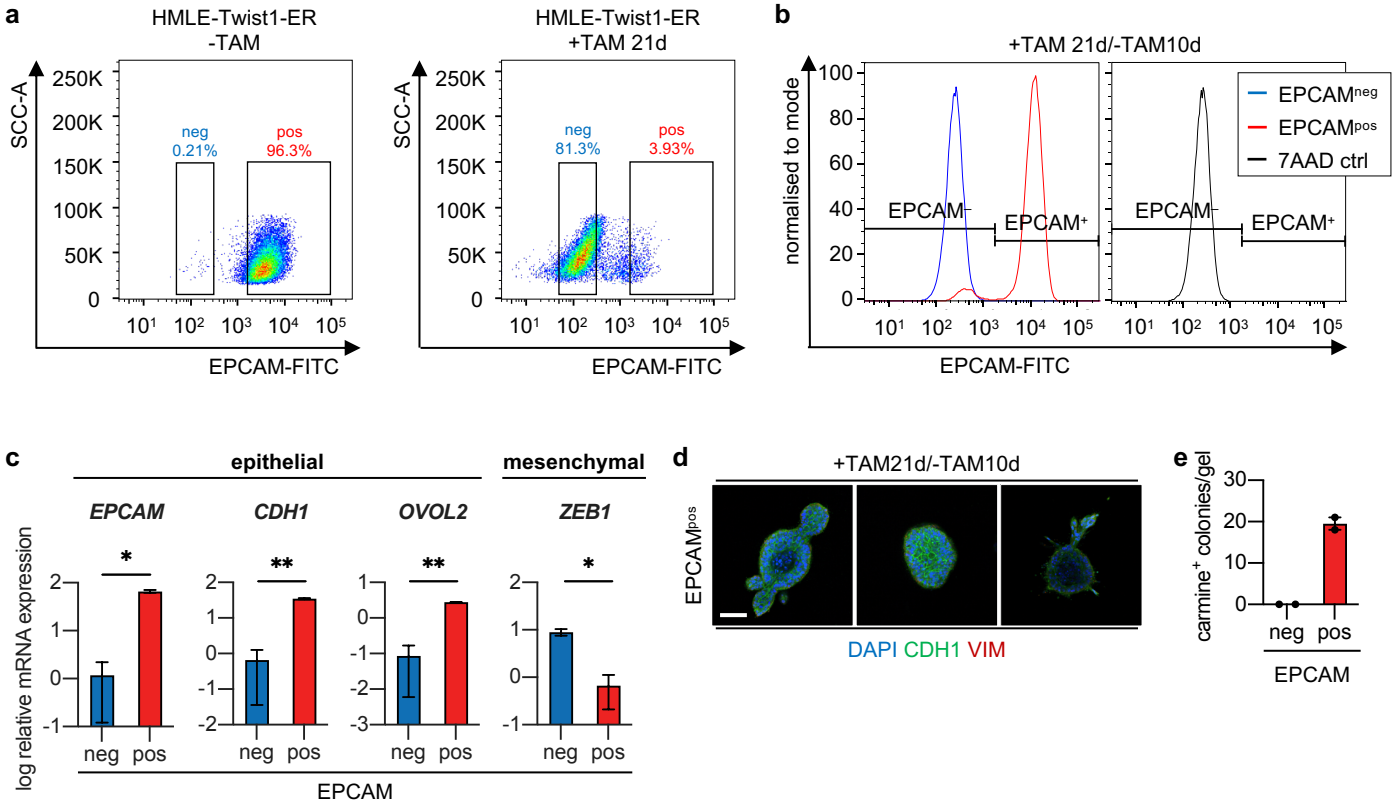

**Figure 3: A subset of breast cancer single-cell clones resists complete EMT and maintains the ability to proliferate in different environments**

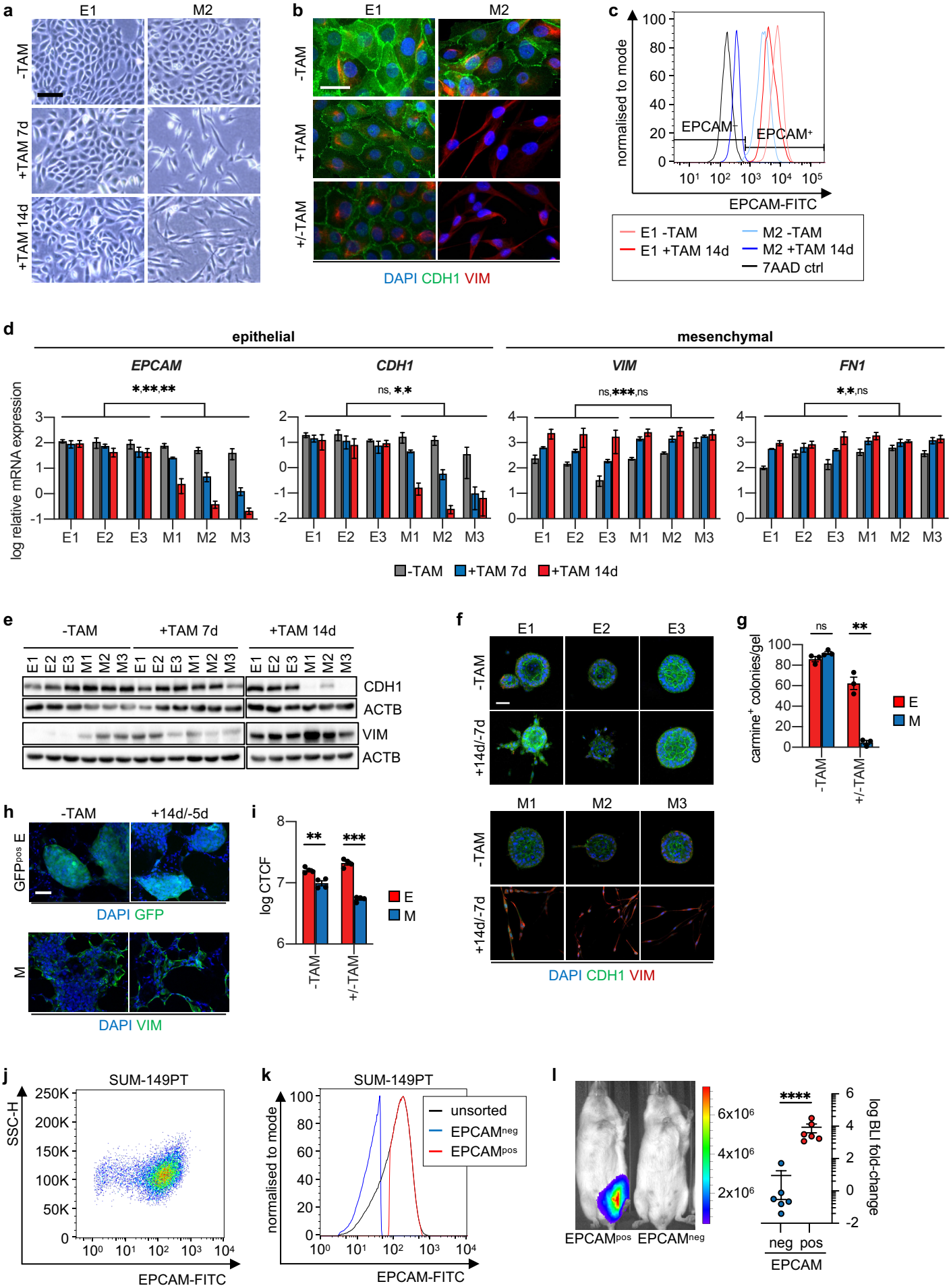

## Figure 4: EMT-induction causes genome-wide chromatin and transcriptional changes

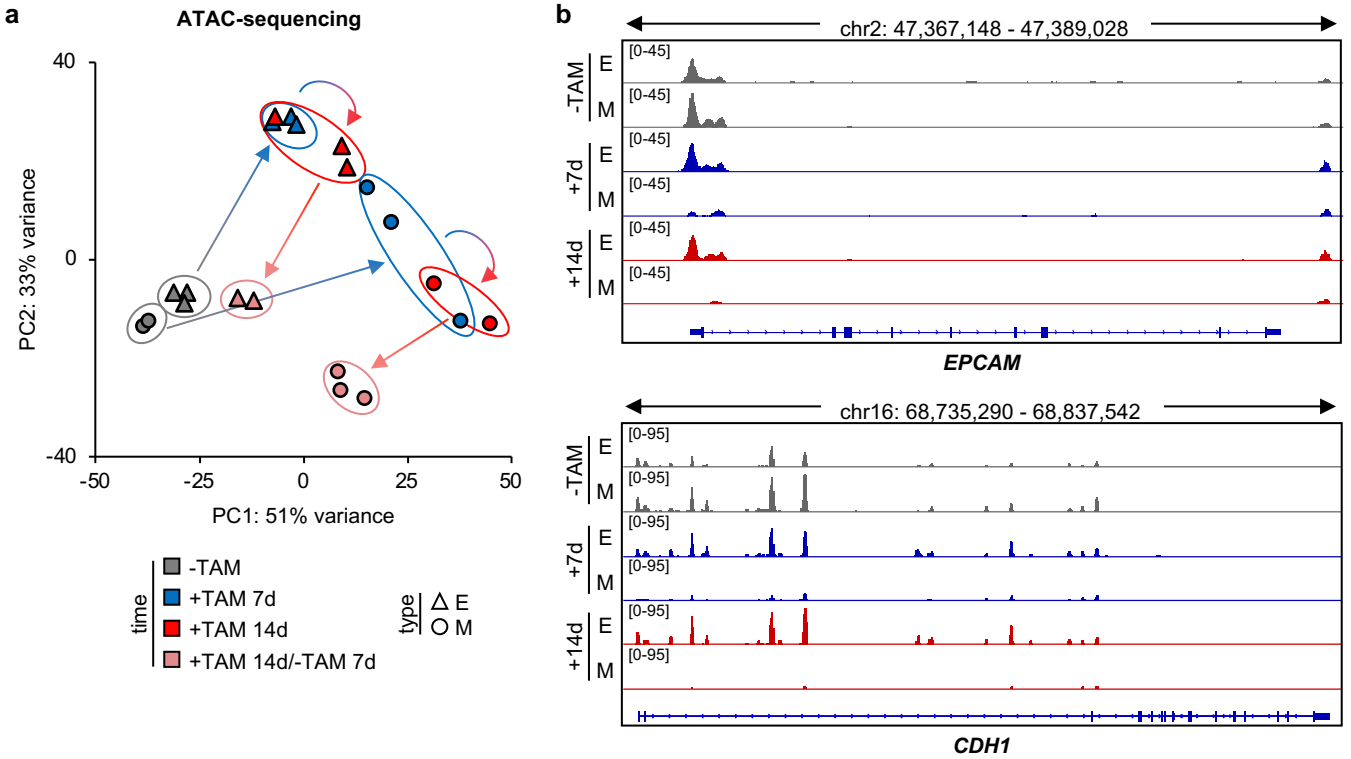


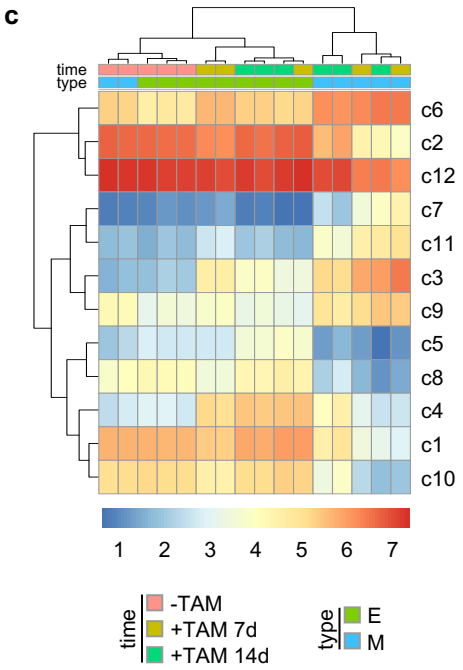


d

| closing exclusively in M during +TAM (c2, c12, c5, c8, c1, c10) | Rank | Motif | P-value | % of Targets | % of Background | Best match Rank1 | Best match Rank 2 |
|---|---|---|---|---|---|---|---|
| | 1 | | 1E-3737 | 41.56% | 5.68% | Fra1 | JunB |
| | 2 | | 1E-753 | 35.51% | 16.18% | **GRHL1** | **GRHL2** |
| | 3 | | 1E-660 | 26.98% | 11.07% | **ZEB1** | **ZEB2** |
| | 4 | | 1E-475 | 25.11% | 11.62% | KLF5 | KLF6 |
| | 5 | | 1E-433 | 14.61% | 5.12% | p53 | p73 |

**Figure 5: The EMT-transcription factor ZEB1 is required for EMT, but not sufficient to overcome EMT-resistance**

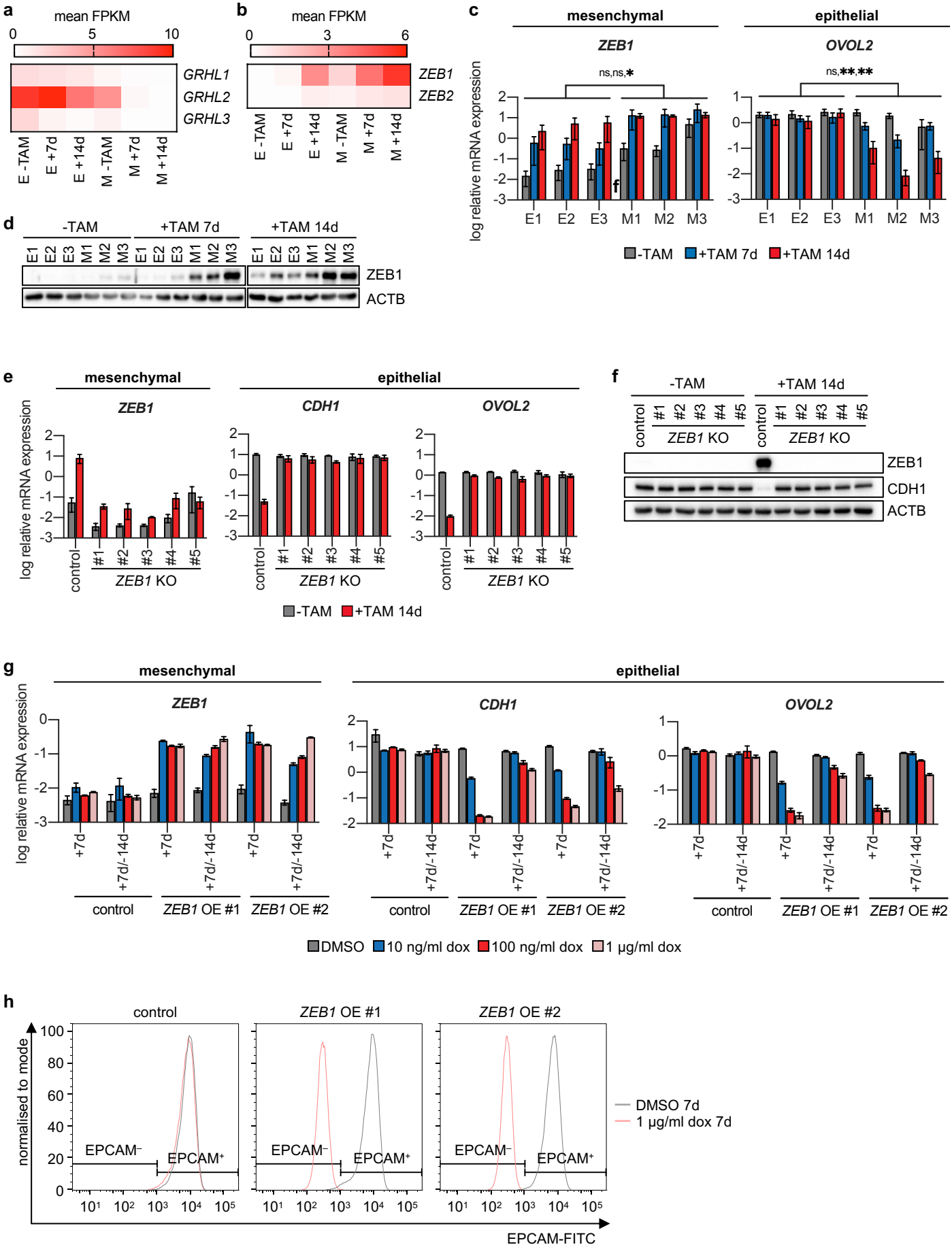

## Figure 6: Maintenance of epithelial features promotes metastatic outgrowth

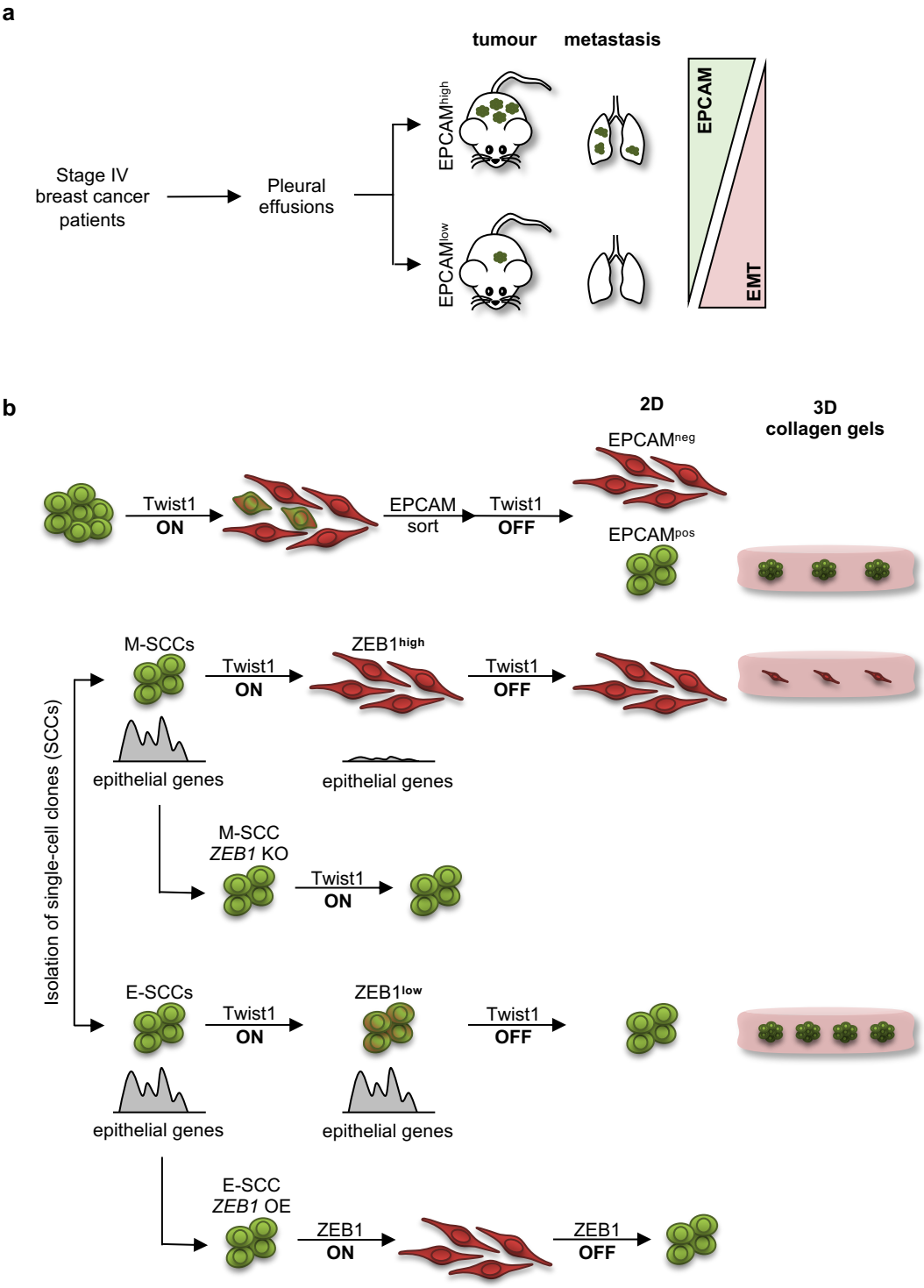

## Supplementary Figure 1: High EPCAM expression correlates with disease-propagating potential in metastatic breast cancer cells

**a**

| Patient | Stage | ER | Clinical subtype | Histology type | TNM classification |
|---|---|---|---|---|---|
| #1 | IV | neg (-) | Triple negative | I. invasive lobular carcinoma | cT4d cNx cM1 |
| #2 | IV | pos (+) | Luminal | I. invasive lobular carcinoma | pT3(m) pN3a M1 |
| #3 | IV | pos (+) | Luminal B | I. invasive ductal carcinoma | ypT4 pN1 M0 |
| #4 | IV | neg (-) | Triple negative | I. invasive mammary carcinoma | pT2 pN0 M0 |
| #5 | IV | pos (+) | Luminal | I. invasive ductal carcinoma | pT3 pN1a(1/13) M0 |
| #6 | IV | pos (+) | Luminal A | I. invasive lobular carcinoma | pT2 pN1a(1/8) cM0 |
| #7 | IV | pos (+) | Luminal B | I. invasive ductal carcinoma | pT1 N0(0/13) cM0 |
| #8 | IV | pos (+) | Claudin-Low | I. invasive mammary carcinoma | pT1b(m) pN1b(2/16) 0/5 |
| #9 | IV | pos (+) | Luminal | I. invasive mammary carcinoma | pT4b pN1 cM0 |
| #10 | IV | neg (-) | Triple negative | I. invasive ductal carcinoma | pT1c pN3a(21/22) cM0 |

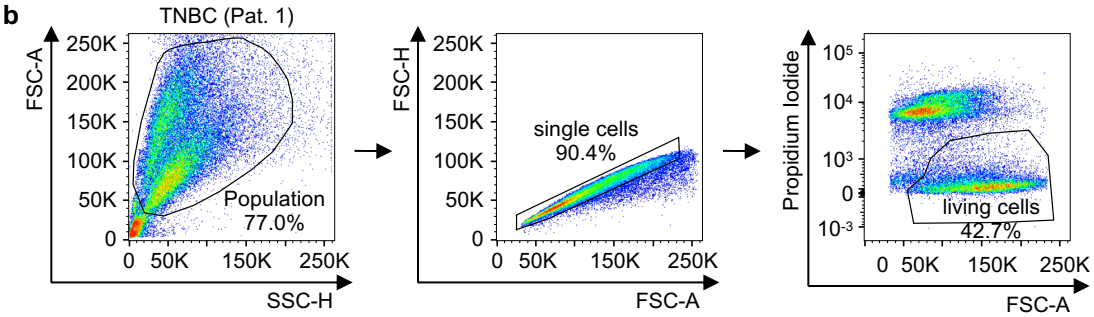


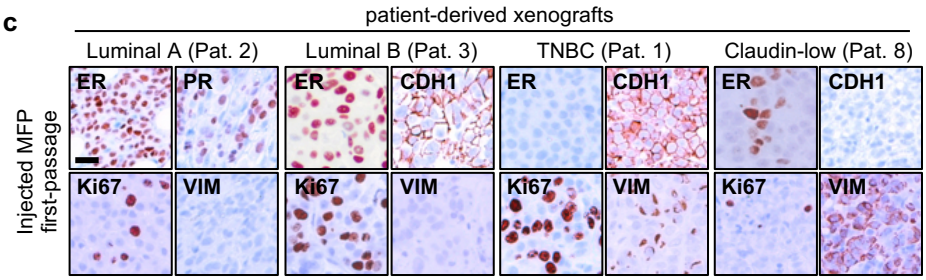


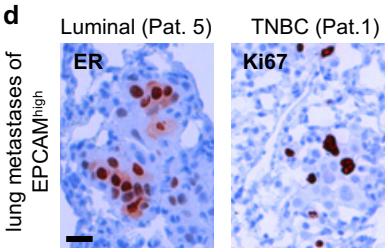


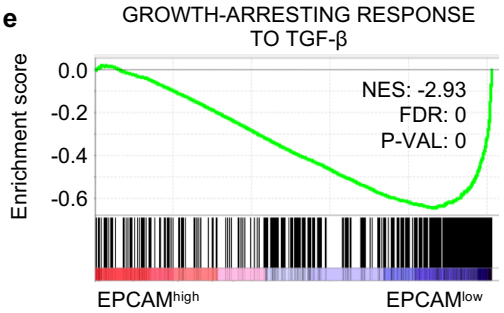


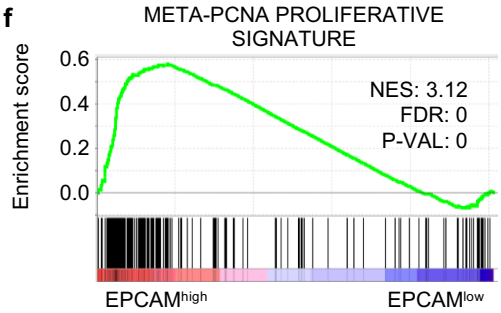

**Supplementary Figure 2: A subset of HMLE-Twist1-ER cells maintains EPCAM expression during EMT-induction**

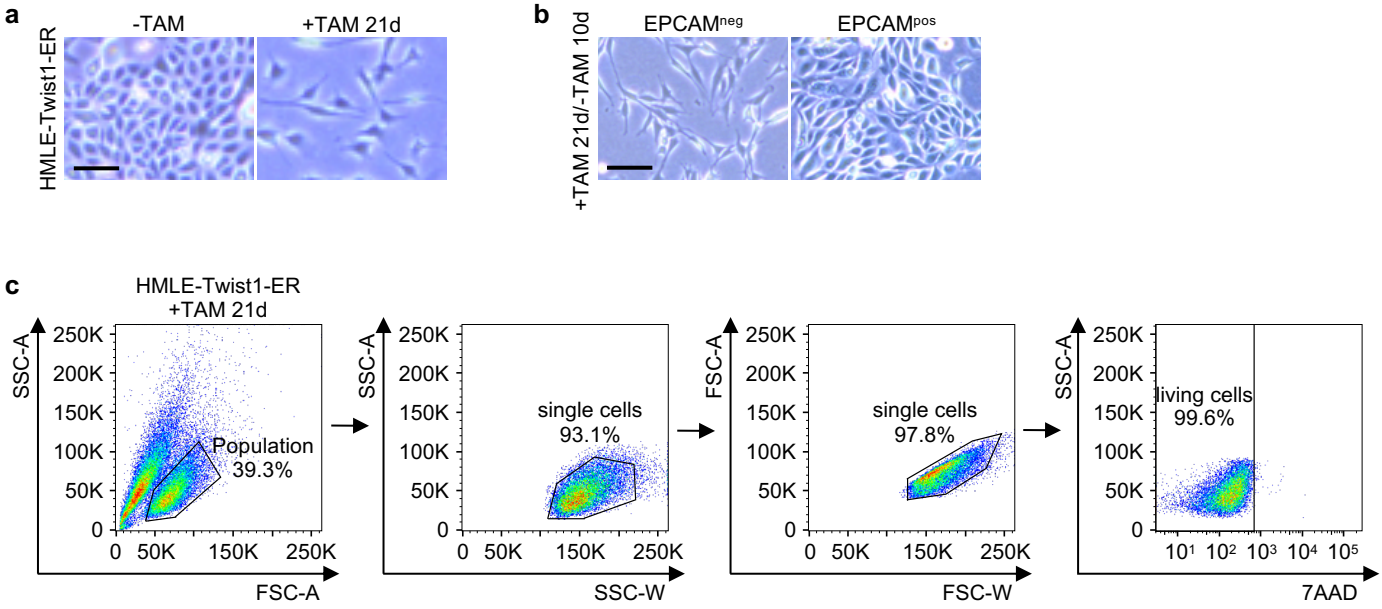

**Supplementary Figure 3: A subset of breast cancer single-cell clones resists complete EMT and maintains the ability to proliferate in different environments**

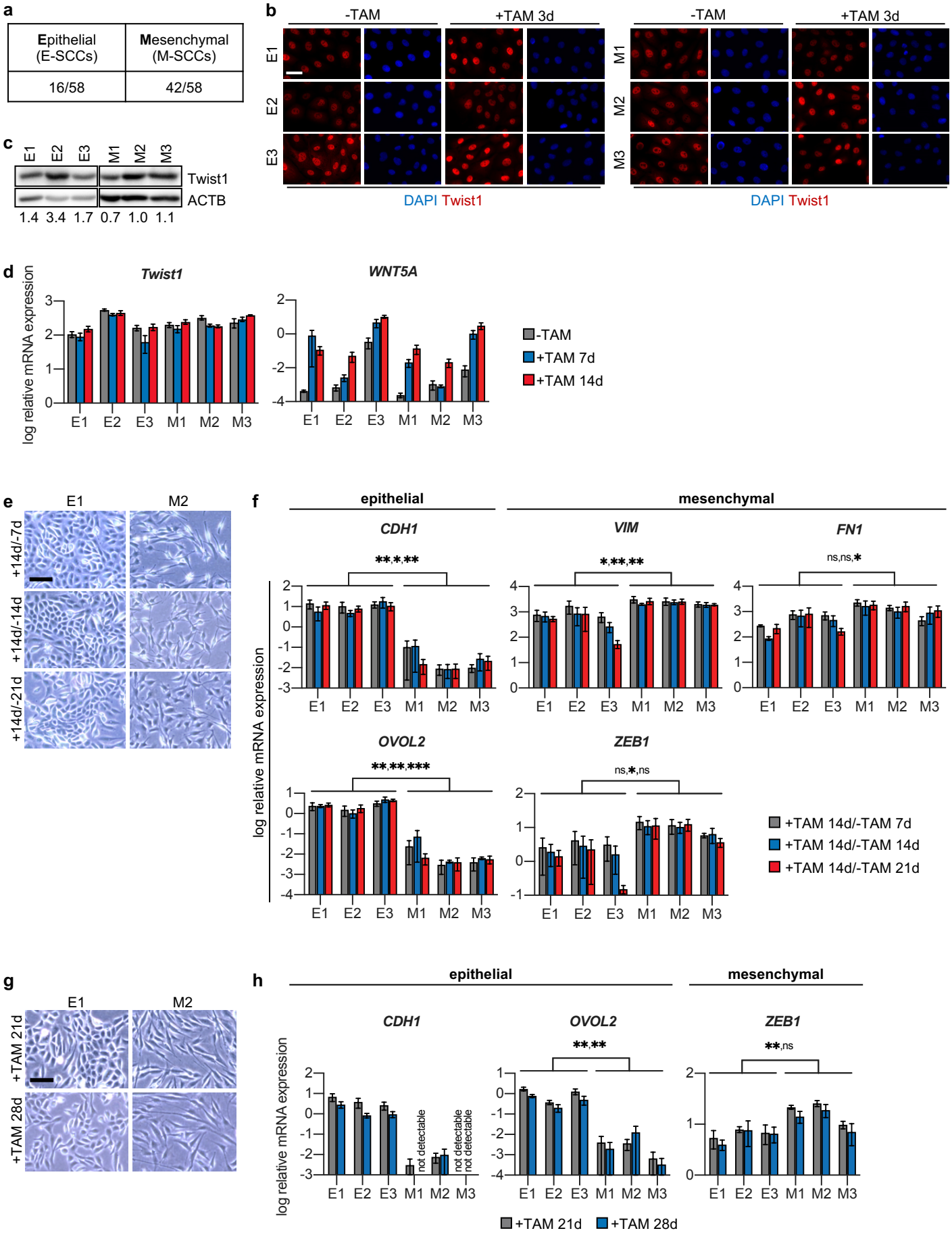

**Supplementary Figure 4: EMT-induction causes genome-wide chromatin and transcriptional changes**

**a**

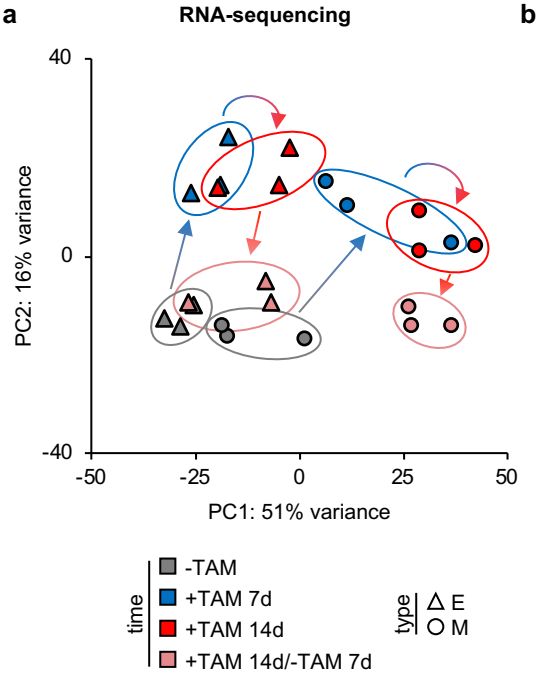


**b**

| | Rank | Motif | Name | P-value | % of Target Sequences with Motif | % of Background Sequences with Motif |
|---|---|---|---|---|---|---|
| opening in M and E during +TAM (c3, c4) | 1 | 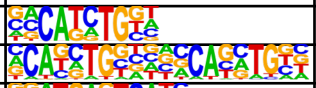 | TCF4 | 1E-370 | 0.5574 | 0.2005 |
| | 2 | | Twist | 1E-360 | 0.191 | 0.0174 |
| | 3 | | Fra1 | 1E-341 | 0.2651 | 0.0438 |
| | 4 | 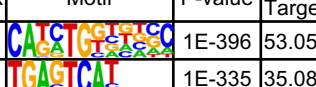 | Atf3 | 1E-340 | 0.2938 | 0.0558 |
| | 5 | 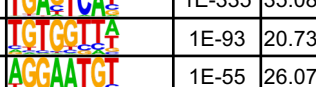 | JunB | 1E-323 | 0.2614 | 0.0453 |

| | Rank | Motif | P-value | % of Targets | % of Background | Best match Rank1 | Best match Rank 2 |
|---|---|---|---|---|---|---|---|
| opening in M and E during +TAM (c3, c4) | 1 | 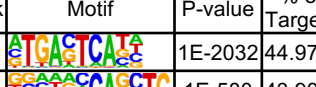 | 1E-396 | 53.05% | 17.26% | TCF4 | Atoh1 |
| | 2 | | 1E-335 | 35.08% | 8.36% | FOSL2::JUN | AP-1 |
| | 3 | 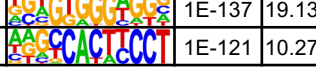 | 1E-93 | 20.73% | 8.15% | RUNX | RUNX1 |
| | 4 |  | 1E-55 | 26.07% | 14.57% | TEAD2 | TEAD1 |
| | 5 |  | 1E-38 | 11.44% | 5.11% | KLF3 | KLF5 |

| | Rank | Motif | P-value | % of Targets | % of Background | Best match Rank1 | Best match Rank 2 |
|---|---|---|---|---|---|---|---|
| Opening exclusively in M during +TAM (c6, c7, c11, c9) | 1 |  | 1E-2032 | 44.97% | 7.05% | BATF | Atf3 |
| | 2 |  | 1E-580 | 43.90% | 19.39% | TCF4 | Ascl1 |
| | 3 |  | 1E-144 | 6.51% | 1.78% | PGR | GRE |
| | 4 |  | 1E-137 | 19.13% | 10.13% | WT1 | Egr2 |
| | 5 |  | 1E-121 | 10.27% | 4.26% | ETS:RUNX | PU.1 |
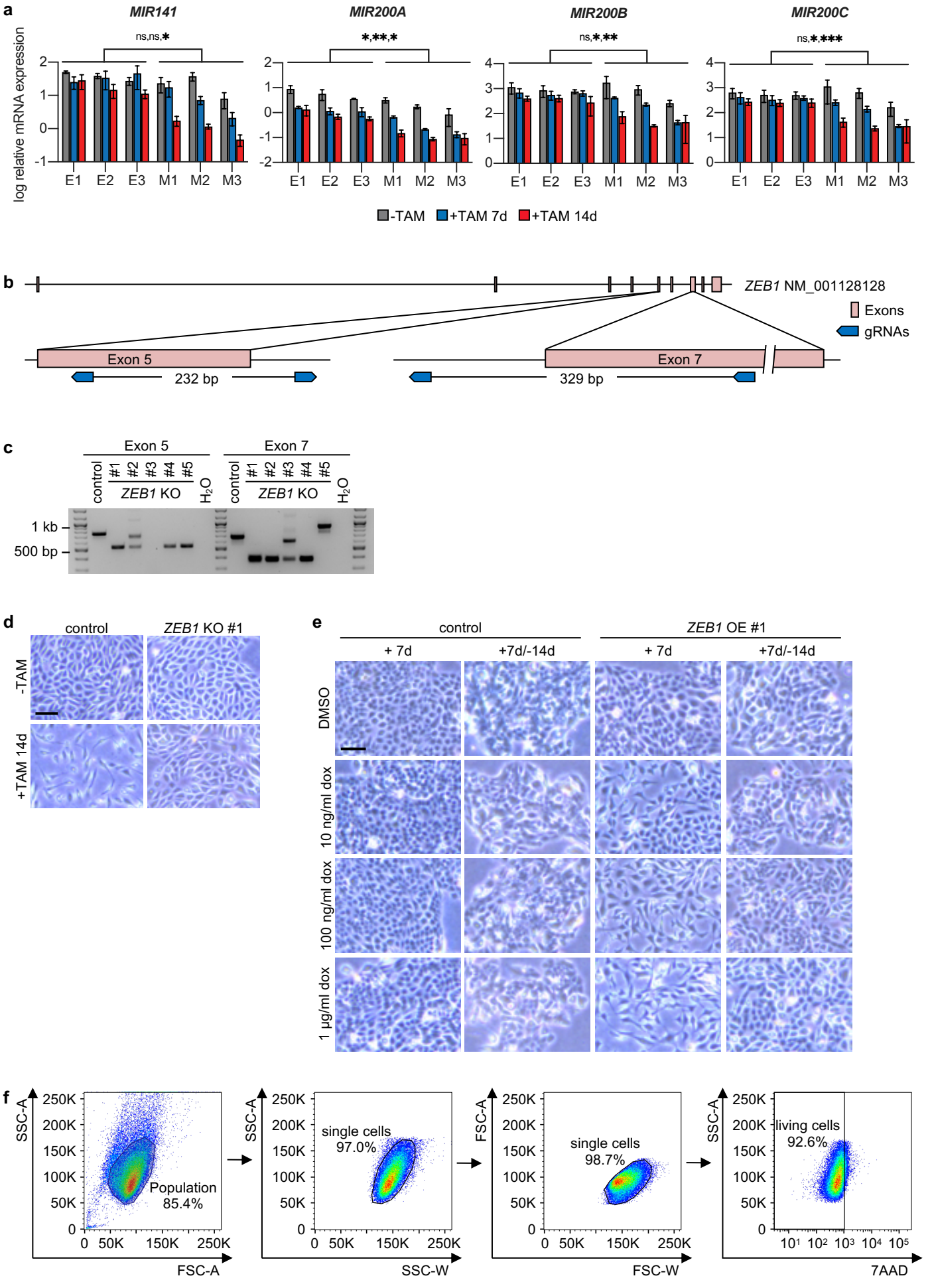
**Supplementary Figure 5: The EMT-transcription factor ZEB1 is required for EMT, but not sufficient to overcome EMT-resistance**